MASTER

Assesment of the Baer-Nunziato seven-equation model applied to steam-water transients calibration of the stiffened gas equation of state based on steam-water tables

van de Leur, L.S.

Award date:
2015

Eindhoven University of Technology
Department of Mathematics and Computer Science

Assessment of the Baer-Nunziato Seven-Equation Model Applied to Steam-Water Transients

Calibration of the Stiffened Gas Equation of State based on Steam-Water Tables

Master Thesis

Lotte van de Leur

Supervisors:
dr.ir. F. Daude (EDF)
prof.dr.ir. B. Koren (TU/e)
dr.ir. A.S. Tijsseling (TU/e)

Eindhoven, September 2015

Abstract

This thesis concerns the simulation of so called water hammers. Water hammers are pressure waves propagating through pipes filled with water. These pressure waves are created when the flow of water in a pipe is suddenly stopped, and can cause severe damage on the structure.

Électricité de France (EDF) is a French electricity company. In the power plants of EDF water hammers occur. Due to safety regulations, if such a water hammer occurs the system has to be shut down.

The water hammers are simulated to get a better understanding of the phenomenon. This will be used to reduce the downtime of the system and eventually prevent water hammers from occurring. For the simulation a two-fluid model is used. In this research project a new calibration of the equation of state coefficients is proposed. These coefficients are used in the calculations of the model. The model with the new calibration of the coefficients is assessed by comparing results of the model to experimental data and numerical results of other models.

The results on the experiments of the seven-equation model are similar to the results of other numerical models. When comparing them to the experimental data some errors are visible. To improve the results the movement of the structure should be included in the model.

Preface

This thesis is a result of my graduation project that I have worked on at the research and development department of EDF. I am grateful to EDF for the opportunity to work on a project in Paris, I found it a very interesting subject and I really enjoyed my time there.

First of all I would like to thank my tutor, Frédéric Daude and PhD student Hippolyte Lochon for helping me during my project. Your constructive feedback, critical questions, patience and willingness to answer my questions gave me confidence and stimulated me during my entire project. Moreover, your company and funny jokes made my stay at EDF very pleasant.

I would like to thank my supervisors from the Eindhoven University of Technology, Arris Tijsseling and Barry Koren, for the guidance during my project. You introduced me to EDF and made it possible for me to study abroad.

Furthermore, I want to thank my colleagues and new friends at EDF for the nice and pleasant work environment, and also for the great times we spend outside of EDF. And I want to thank my friends from the Netherlands who came to visit me during my internship.

Last, but not least I would like to thank my parents, sister and Edwin. I am very grateful for the conversations we had over Skype where you encouraged me and helped me by discussing about my work at EDF. I am glad that I can always count on you. But most of all, I am thankful for your support, encouragement and the interest you showed in me during my entire studies.

Contents

Chapter 1

Introduction

This thesis is the result of a master graduation project carried out by the Eindhoven University of Technology in collaboration with Électricité de France (EDF).

1.1 Électricité de France

EDF is the largest European electricity company that produces electricity primarily from nuclear power. It is a private company with the French government as the largest shareholder (85%). EDF is situated over different countries in Europe, America, Asia and Africa with its headquarter in Paris.

This research project has been conducted in the department of Analysis, Mechanics and Acoustics (Analyses, Mécaniques et Acoustique, AMA) in Paris. The department develops modelling tools and carries out numerical and physical experiments. The topics that they work on are acoustics, mechanical vibration and the mechanical behaviour of structures.

1.2 Project description

Water hammers are pressure waves propagating through pipes. These are caused by a sudden stop of the water flow or when vapour suddenly condensates. In the power plants of EDF about one or two times a year a water hammer incident occurs, specifically in the pipes of the system where the steam condensates to water. When such a water hammer occurs, the system needs to be shut down for safety reasons, to check whether the structure is still intact. This causes the system to be shut down for 30 to 60 days per year, which costs about one million euros per day.

Many models exist to simulate the dynamics of fluids. A distinction can be made between single-phase flow models, two-phase homogeneous models and two-fluid models. The single-phase flow models can only be used for the flow of one phase. In the case of the modelling of water hammers it simulates the flow of water in liquid phase only. The two-phase homogeneous models are used for the flow of two phases of a material as a mixture and models the mixture as a single-phase flow. In the modelling of water hammers, the two-phase homogeneous model simulates the flow of a liquid-vapour mixture. The most complex models are the two-fluid models. In this model the flow of the two different phases, liquid and vapour, are simulated separately. In this research the focus lies on a two-fluid model.

A two-fluid model is constructed, the seven-equation Baer-Nunziato model [1], to simulate water hammers. It is used to get a better understanding of the physics that are involved, and to eventually prevent water hammers from occurring in the EDF facilities. And when such a water hammer occurs the model can locate the highest pressure peak, such that a smaller part of the

system needs to be checked, which will reduce the downtime.

In the current systems of the power plants the water hammers cannot be measured. Therefore the seven-equation model is assessed using experiments that have been simulated or executed before. The results of the model are compared with experimental data and results of other verified models. The seven-equation model is implemented in Europlexus, a simulation software for fast transient dynamics including fluid-structure interaction, to produce the numerical predictions of the experiments. The goal is to validate different parts of the model.

1.3 Thesis outline

The next chapter, Chapter 2, will give a general explanation of water hammers. This is done with the derivation of the Joukowsky formula which is then applied to the Simpson experiment. The Simpson experiment is chosen because of its simple geometry.

In Chapter 3 the two-phase models are discussed with the two different types of models, namely the homogeneous ones and the two-fluid ones. And more in-depth information is given about the seven-equation model including the relaxation terms belonging to this model.

In Chapter 4 the required equation of state is presented. For the coefficients of the equation of state a new calibration is proposed.

Chapter 5 gives the numerical approximation of the seven-equation model which is implemented and used within Europlexus.

In Chapter 6 the seven-equation model, its relaxation terms and the new calibration of the equation of state coefficients are assessed using Europlexus. To verify the seven-equation model some experiments are simulated with the model and the results are compared with the results of physical experiments and results of other models.

Finally in Chapter 7 the conclusions of the project are drawn and some recommendations for further research on this topic are given.

Chapter 2

Water hammer phenomenon

A classical water hammer is a pressure wave propagating through a pipe filled with liquid. This can be generated when the liquid flowing through a pipe is suddenly stopped. The kinetic energy of the flowing fluid is then converted into a pressure wave. This can occur when a valve is suddenly closed or opened, or when a pump is turned off or on.

Another more complex type of water hammer is the condensation induced water hammer. This type of water hammer occurs when a pipe is filled with water and vapour. When the pressure in the vapour part suddenly increases, for instance by a pressure wave, and when it reaches the saturation pressure, the vapour part suddenly condensates and collapses into liquid water. This collapse causes a pressure wave. Another cause of such a condensation induced water hammer is when a pipe is filled with cold liquid water and hot vapour. Due to the temperature difference the vapour starts to condensate. This causes some instability in the flow and when a hot vapour bubble is surrounded by cold liquid, the bubble collapses into liquid. Again this collapse causes a pressure wave, or a so called water hammer.

In many industries, such as the production of energy, fluid dynamics plays an important role. In these systems water hammers can cause severe damage on pipes. Therefore many research has been done on the water hammer phenomenon. Some well known research in this field has been performed by N. Joukowsky [2]; he formulated the Joukowsky formula that represents the influence of the change in velocity of the liquid on the pressure change, and L. Allievi [3, 4] who found the Allievi equations to model a single-phase flow.

One example (of many) of a catastrophic water hammer accident is presented by Sinha et al. [5]. In this accident a steam main in downtown New York was ruptured and created a cavity of 10 m $\times$ 10 m and 5 m deep, as a result of a condensation induced water hammer. That day, due to heavy rainfall and defects in the sewer and catch basin facilities, the steam main was surrounded by more water then usually. The contact of the water with the pipe wall cooled the steam inside the pipe, this caused the steam to condensate rapidly. The condensate in the pipe blocked the flow of the steam and a steam bubble surrounded by condensate appeared. When the bubble collapsed it caused a water hammer that ruptured the pipe and created the cavity. The effects of the accident are shown in Figure 2.1.

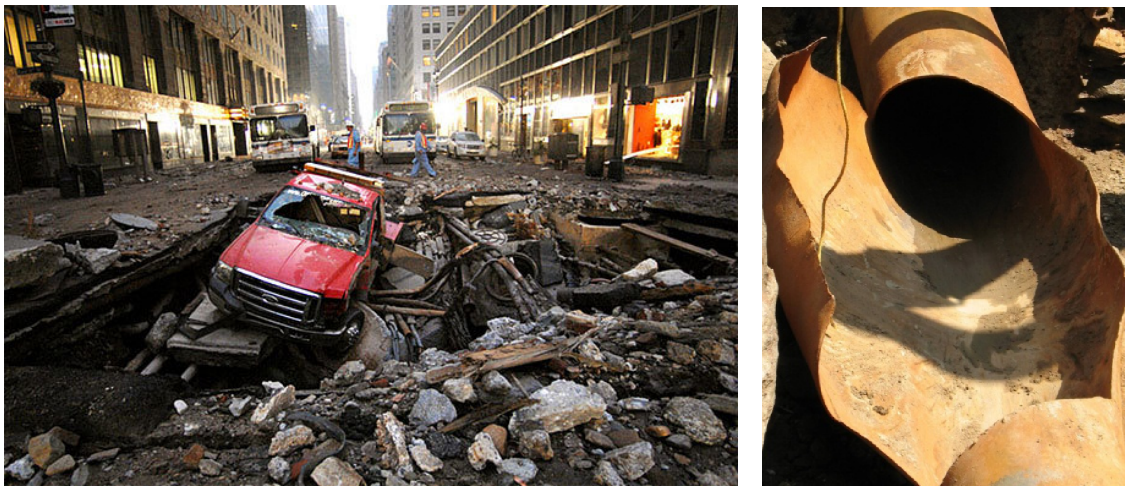

Figure 2.1: Results of the water hammer accident in New York, 2007. Left the cavity that was formed by the explosion and right the ruptured pipe.

2.1 Water hammer theory

To get a global understanding on how water hammers occur, the Joukowsky formula [2] is derived from a simple, two-equation water hammer model, which describes inviscid, single-phase, liquid flows. This model uses one equation for the mass conservation and one equation for the balance of momentum:

$$\begin{cases} \partial_t \rho + \partial_x(\rho u) & = 0 \\ \partial_t(\rho u) + \partial_x(\rho u^2 + p) & = 0 \end{cases} . \tag{2.1}$$

The equation of state is $p = p(\rho)$, where $\frac{\mathrm{d}p}{\mathrm{d}\rho} = \frac{K}{\rho} = c^2 = \text{constant} > 0$, where K is the bulk modulus of the liquid, ρ the density and c the speed of sound. Furthermore $u << c$.

If smooth solutions are considered the equations can be rewritten in terms of the primitive variables, velocity u and pressure p, as follows:

$$\begin{cases} \partial_t \rho + \rho \partial_x u + u \partial_x \rho & = 0 \\ u\left[\partial_t \rho + \partial_x(\rho u)\right] + \rho \partial_t u + \rho u \partial_x u + \partial_x p & = 0 \end{cases} . \tag{2.2}$$

Using the first equation of (2.1) the part between the square brackets can be eliminated,

$$\begin{cases} \partial_t \rho + \rho \partial_x u + u \partial_x \rho & = 0 \\ \rho \partial_t u + \rho u \partial_x u + \partial_x p & = 0 \end{cases} . \tag{2.3}$$

Using the equation of state $\partial_t \rho = \frac{\mathrm{d}\rho}{\mathrm{d}p} \partial_t p = \frac{1}{c^2} \partial_t p$ the model becomes

$$\begin{cases} \frac{1}{c^2} \partial_t p + \rho \partial_x u + u \partial_x \rho & = 0 \\ \rho \partial_t u + \rho u \partial_x u + \partial_x p & = 0 \end{cases} . \tag{2.4}$$

Because $u << c$ the terms $u\partial_x \rho$ and $\rho u \partial_x u$ are not significant compared to the other terms. Therefore they can be removed from the equation,

$$\begin{cases} \frac{1}{c^2} \partial_t p + \rho \partial_x u & = 0 \\ \rho \partial_t u + \partial_x p & = 0 \end{cases} , \tag{2.5}$$

and this is rewritten to

$$\begin{cases} \partial_t p + \rho c^2 \partial_x u & = 0 \\ \partial_t u + \frac{1}{\rho} \partial_x p & = 0 \end{cases} . \tag{2.6}$$

These equations are the water hammer equations or also called the Allievi equations [3, 4] without friction between the walls and the fluid. Now the model can be written in the matrix-form

$$\partial_t W + B\partial_x W = 0, \tag{2.7}$$

where

$$W = \begin{pmatrix} p \\ u \end{pmatrix} \quad \text{and} \quad B = \begin{pmatrix} 0 & \rho c^2 \\ 1/\rho & 0 \end{pmatrix}.$$

The eigenvalues of matrix B are the velocities of the waves present in the system, in this case $-c$ and c.

Note that in the liquid single-phase system the wave speed c and the density ρ are constant. So to find the Joukowsky equation from Equation (2.7), it can be rewritten as

$$\begin{aligned} & \partial_t W + B\partial_x W = 0 \\ \Leftrightarrow \quad & \partial_t W + \partial_x BW = 0 \\ \Leftrightarrow \quad & \partial_t W + \partial_t BW \ \frac{\mathrm{d}t}{\mathrm{d}x} = 0. \end{aligned} \tag{2.8}$$

Now the jump over time of value ξ is denoted as $\Delta\xi$, and using the fact that $\frac{\mathrm{d}t}{\mathrm{d}x} = \pm\frac{1}{c}$ the above equation gives

$$\begin{aligned} \Delta\left(BW\right) &= \pm c\Delta W \\ \Delta \begin{pmatrix} \rho c^2 u \\ p/\rho \end{pmatrix} &= \pm c\Delta \begin{pmatrix} p \\ u \end{pmatrix} \\ \begin{pmatrix} \rho c^2 \Delta u \\ \frac{1}{\rho}\Delta p \end{pmatrix} &= \pm c \begin{pmatrix} \Delta p \\ \Delta u \end{pmatrix}. \end{aligned}$$

Thus the Joukowsky formula is obtained;

$$\Delta p = \pm \rho c \Delta u, \tag{2.9}$$

where $\pm$ depends on the direction of the pressure wave. With this simple equation the pressure magnitude of a water hammer can be calculated.

2.2 Influence of the pipe elasticity

The water hammer model can be extended to include the elasticity of the pipe wall. For this purpose the cross section of the pipe $A(x,t)$ is introduced. This is added to the water hammer model as follows:

$$\begin{cases} \partial_t(\rho A) + \partial_x(\rho u A) & = 0 \\ \partial_t(\rho u A) + \partial_x(\rho u^2 A + pA) & = p\partial_x A \end{cases}, \tag{2.10}$$

where in this case ρ, u and p are the average values of the density, velocity and the pressure over the cross section of the pipe; A. Again $p = p(\rho)$ such that $\frac{\mathrm{d}p}{\mathrm{d}\rho} = c^2 = \text{constant} > 0$ and $A = A(p)$ due to the hoop elasticity. When the material and geometrical properties of the pipe are included, the equation $\frac{\mathrm{d}A}{\mathrm{d}p} = \frac{AD}{Ed}$ is retrieved, where D is the inner diameter of the pipe, d the thickness of the wall of the pipe and E the Young's modulus of the material of the pipe. See for these equations also the article on water hammer theory by Ghidaoui et al. [6].

If smooth solutions are considered the first equation of (2.10) can be rewritten in terms of the primitive variables u and p. The first equation is

$$A\partial_t\rho + \rho\partial_t A + \rho u\partial_x A + Au\partial_x\rho + A\rho\partial_x u = 0. \tag{2.11}$$

Because $u << c$ the terms $\rho u \partial_x A$ and $A u \partial_x \rho$ are not significant compared to the other terms and are therefore eliminated,

$$A\partial_t \rho + \rho \partial_t A + A\rho \partial_x u = 0. \tag{2.12}$$

Substitute $A\partial_t \rho = A\frac{\mathrm{d}\rho}{\mathrm{d}p}\partial_t p$ and $\rho \partial_t A = \rho \frac{\mathrm{d}A}{\mathrm{d}p}\partial_t p$ and divide by A,

$$\begin{aligned} &\left(\frac{\mathrm{d}\rho}{\mathrm{d}p} + \frac{\rho}{A}\frac{\mathrm{d}A}{\mathrm{d}p}\right)\partial_t p + \rho \partial_x u = 0 \\ &\left(\frac{1}{c^2} + \frac{\rho}{A}\frac{AD}{Ed}\right)\partial_t p + \rho \partial_x u = 0 \\ &\frac{1}{\tilde{c}^2}\partial_t p + \rho \partial_x u = 0, \end{aligned} \tag{2.13}$$

where Korteweg's formula [7] for the adjusted celerity is

$$\begin{aligned} \frac{1}{\tilde{c}^2} &= \frac{1}{c^2} + \frac{\rho D}{Ed} = \frac{1 + \rho c^2 \frac{D}{Ed}}{c^2} \\ \tilde{c}^2 &= \frac{c^2}{1 + \rho c^2 \frac{D}{Ed}} = \text{constant} > 0. \end{aligned} \tag{2.14}$$

The values ρ, c^2, D, d and E are all positive, so it follows that $\tilde{c}^2 < c^2$ and thus the speed of the wave is lower when the hoop flexibility of the pipe is considered.

The second equation of (2.10) can be rewritten for smooth solutions into

$$\begin{aligned} &u\partial_t(\rho A) + \rho A \partial_t u + u\partial_x(\rho u A) + \rho u A \partial_x u + p\partial_x A + A\partial_x p = p\partial_x A \\ &u\partial_t(\rho A) + \rho A \partial_t u + u\partial_x(\rho u A) + \rho u A \partial_x u + A\partial_x p = 0. \end{aligned} \tag{2.15}$$

Because $u << c$ and the deformation of the pipe is assumed to be very small, the terms $u\partial_t(\rho A)$, $u\partial_x(\rho u A)$ and $\rho u A \partial_x u$ are ignored. Then the whole equation is divided by ρA and becomes

$$\partial_t u + \frac{1}{\rho}\partial_x p = 0. \tag{2.16}$$

So the system is reduced to

$$\begin{cases} \partial_t p + \rho \tilde{c}^2 \partial_x u &= 0 \\ \partial_t u + \frac{1}{\rho}\partial_x p &= 0 \end{cases}. \tag{2.17}$$

This is equivalent to the system of the rigid pipe, but now with the adjusted squared celerity $\tilde{c}^2 < c^2$. Also for this case the Joukowsky equation can be derived as

$$\Delta p = \pm \rho \tilde{c} \Delta u, \tag{2.18}$$

for $\tilde{c} = \frac{c}{\sqrt{1+\rho c^2 \frac{D}{Ed}}} = \frac{c}{\sqrt{1+K\frac{D}{Ed}}}$, where K is the bulk modulus of the single-phase liquid. Note that $\tilde{c} < c$, so that the jump of pressure will be smaller in the case where the flexibility of the pipe is taken into account.

So again the simple Joukowsky formula is retrieved with an adjusted lower wave speed to represent the elasticity of the pipe.

2.3 Application to the Simpson experiment

To get a better understanding of a water hammer propagating through a pipe, the Joukowsky formula is used for the computation of the pressure history in the Simpson experiment [8, 9].

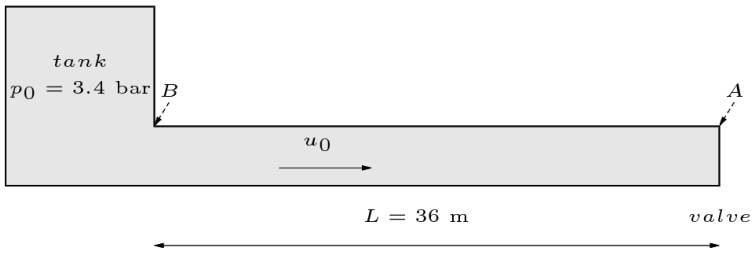

Figure 2.2: The model of the Simpson experiment.

The Simpson experiment is an experiment with a simple geometry, see Figure 2.2; it concerns a straight pipe filled with water in liquid phase. One end of the pipe is attached to a tank filled with water under a constant pressure $p_0 = 3.419$ bar. The water flows from the tank with a constant velocity u_0 through the pipe. At time $t = 0$ a valve, at a distance $L = 36$ m from the tank, is rapidly closed. This creates a water hammer where the pressure wave propagates in the direction opposite of the initial velocity. The height of the pressure jump in the system is calculated using the Joukowsky formula at point A, which is at the valve, and the velocity is calculated at point B, which is at the tank.

The Simpson experiment has been carried out with different initial velocities and this resulted in two entirely different outcomes. The first case is when the initial velocity is $u_0 = 0.239$ m/s; in this case the velocity is not high enough to cause cavitation. This is called the single-phase experiment. And the second case is when the initial velocity is $u_0 = 0.401$ m/s which is high enough to cause cavitation. This case is called the two-phase experiment.

In the single-phase experiment, cavitation does not appear, so the wave will travel undisturbed from the valve to the tank and back to the valve. This process continues until it dies out because of friction (this is not included here). The result of the computation of the pressure at point A using the Joukowsky formula is shown in Figure 2.3.

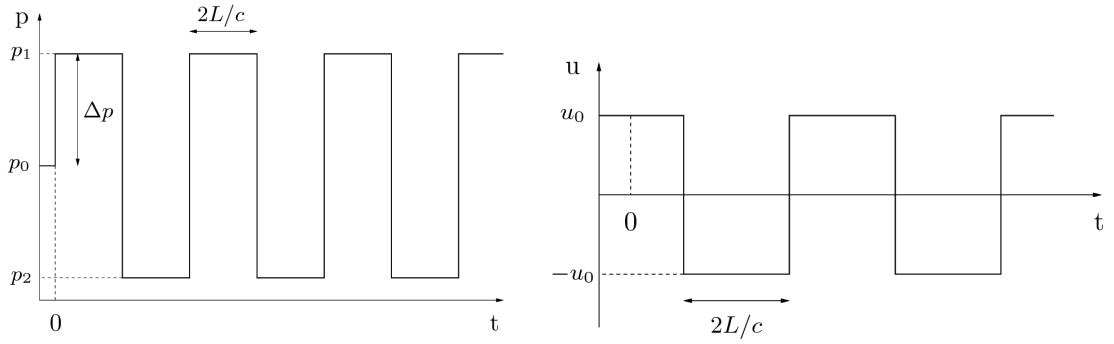

Figure 2.3: Left, the results of the pressure at point A and right the results of the velocity at point B, computed with the Joukowsky formula in the single-phase experiment.

In the two-phase experiment at time $2L/c$ the pressure wave front is located at the valve and will propagate back to the tank. At this moment at point A, the pressure drops. This time the pressure drops to the vapour pressure and cavitation occurs, so a bubble of vapour appears at the valve. Later on, when the pressure in the bubble remains constant at vapour pressure (≈ 0 bar); a second and even stronger water hammer occurs when the liquid hits the closed end; the vapour

bubble collapses.

This two-phase experiment, where a vapour bubble appears at the valve, is again computed using the Joukowsky equation, $\Delta p = \pm \rho c \Delta u$. The velocity of the wave is computed at point B and the pressure profile is computed at point A. The pressure at the tank is kept constant and equal to p_0, and at the closed valve the velocity is constant and equal to zero when there is no vapour bubble. In the calculations ε is used for the time it takes for the vapour bubble to collapse. The value of ε is taken from the experiment, as is Δp_2. The calculations are given in appendix A. Figure 2.4 left shows the evolution of the pressure at point A and right shows the evolution of the velocity in point B. Clearly the propagation of the water hammer is visible.

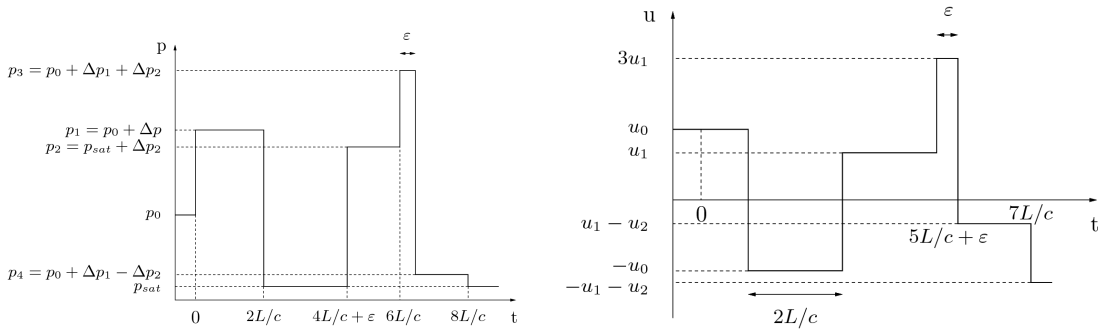

Figure 2.4: Left, the results of the pressure at point A and right the results of the velocity at point B, computed with the Joukowsky formula in the two-phase case.

The measured results of the pressure in the single-phase and two-phase Simpson experiment are shown in Figure 2.5. Here a similar pressure profile can be seen as the profile in Figures 2.3 and 2.4, which were calculated using the Joukowsky formula.

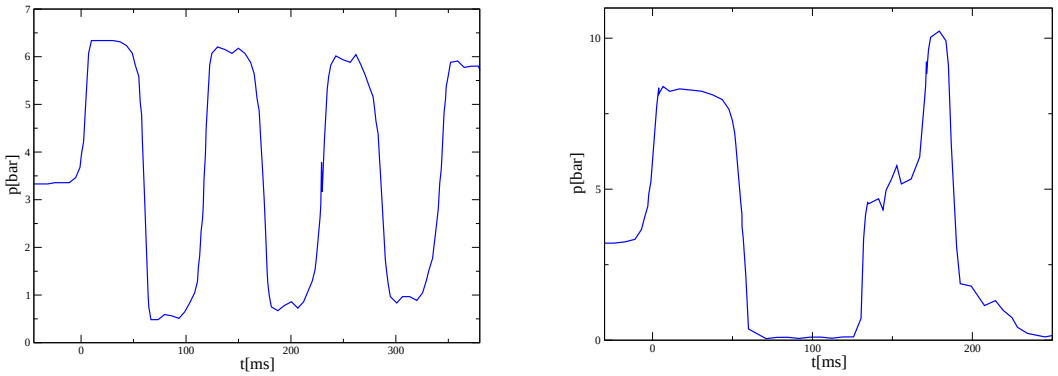

Figure 2.5: Pressure measured at point A of the Simpson experiment. Left the single-phase experiment, right the two-phase experiment.

2.4 Limitations of the single-phase models

The computation of the water hammers using the Joukowsky formula gives good results with some simple assumptions. The main disadvantage of this single-phase model is the assumption of just one phase. When in the model a second phase appears and disappears, for instance by cavitation and condensation, this is not simulated and the model can yield results which do not match the

physics. With some additional input parameters such as the time, ε, it takes for the vapour bubble to collapse when the water front returns to the closed end and the height of the second pressure peak $p_{sat} + \Delta p_2$, the pressure history in the Simpson experiment can be obtained. But to compute the behaviour of the liquid and the vapour in a water hammer where two different phases of water appear, a more complex model is needed. For the modelling of two-phase water hammers a two-phase flow model is required. Relatively simple models exist for isothermal water hammers with cavitation, more information on these models is given in the article of Bergant et al. [10]. In Chapter 3 more advanced models are introduced, which are adequate for steam condensation.

Chapter 3

Two-phase flow models

Substance occurs in three different phases, solid, liquid and gas. A flow where two different phases of a substance occur is called two-phase flow.

To simulate a water hammer, where vapour appears in the pipes, a two-phase flow model is needed. This is a model that simulates a two-phase flow where the phases in this case are liquid and vapour.

The two-phase flow models can be divided into two different types. One type is the homogeneous type, where the liquid and vapour mixture is considered as a single flow. Some equilibria between the two phases are assumed. The other type is called the two-fluid model. In these models the two different phases are modelled separately. One example of a two-fluid model is the well-known seven-equation model; in the sequel the focus lies on this model.

3.1 Seven-equation model

In this research project the two-fluid, seven-equation model [11] is examined. This model is chosen because it is a general and hyperbolic set of equations. It is a two-fluid model where an equilibrium between the two different phases is not assumed. This seven-equation model is an Euler-type model and is given in 1D by ($k = 1, 2$):

$$\begin{cases} \partial_t \alpha_k + u_I \partial_x \alpha_k & = \Phi_k \\ \partial_t(\alpha_k \rho_k) + \partial_x(\alpha_k \rho_k u_k) & = \Gamma_k \\ \partial_t(\alpha_k \rho_k u_k) + \partial_x(\alpha_k \rho_k u_k^2 + \alpha_k p_k) - p_I \partial_x \alpha_k & = \Lambda_k \\ \partial_t(\alpha_k \rho_k e_k) + \partial_x(\alpha_k \rho_k e_k u_k + \alpha_k p_k u_k) - p_I u_I \partial_x \alpha_k & = \Psi_k \end{cases} . \tag{3.1}$$

Although this appears to be eight equations, it will be shown, since there is some dependence, that only seven equations remain. This explains the name of the model. The governing variables are the density ρ_k, the velocity u_k, the pressure p_k, the total specific energy e_k and the volume fraction α_k for $k = 1, 2$, indicating the different phases. Where in the sequel of this research, phase 1 represents the vapour and phase 2 the liquid. The total energy and the specific internal energy of phase k are given respectively by

$$e_k = \varepsilon_k + \frac{1}{2} u_k^2 \tag{3.2}$$

$$\varepsilon_k = \varepsilon_k(\rho_k, p_k). \tag{3.3}$$

The Equation Of State (EOS) is defined by the specific internal energy. Furthermore, the homogeneous part of the model is hyperbolic in the case that $|u_k - u_I| \neq c_k$. The eigenvalues of the hyperbolic seven-equation model are; $u_k, u_I, u_k - c_k$ and $u_k + c_k$ for $k = 1$ and $k = 2$. These eigenvalues correspond to the velocities of the waves occurring in the system. The eigenvalues u_k

are associated to a linear degenerate field, which means that the waves are contact discontinuities. The eigenvalues $u_k \pm c_k$ are associated to a genuinely nonlinear field, which means the waves are rarefaction or shock waves.

The inter-facial quantities are chosen in a way such that the non-conservative terms are not active across the shock waves, as explained in the article by Coquel et al. [12] and the article by Gallouët et al. [13]. In other words, the field associated to the eigenvalue u_I should be linear degenerate. For that purpose they have found three different possible choices for u_I, namely: u_1, u_2 and $\frac{\alpha_1\rho_1u_1+\alpha_2\rho_2u_2}{\alpha_1\rho_1+\alpha_2\rho_2}$. With this choice, p_I is defined by the existence of the entropy for the model.

In research done by Lochon et al. [11] the three different choices are compared with each-other on the Canon experiment. The results show that, when only focusing on the convective part, the numerical results are different (the number of waves present in the system differs per choice). However, when the relaxation terms are included, the numerical results are similar.

In this research project the focus lies on the Baer-Nunziato [14] closure law, and thus the inter-facial quantities are chosen as

$$(u_I, p_I) = (u_2, p_1). \tag{3.4}$$

For the volume fraction of the two phases it holds that

$$\alpha_1 + \alpha_2 = 1, \tag{3.5}$$

therefore for $k = 1$ and $k = 2$ the first equations are dependent, so that one can be eliminated and seven equations remain. The seven-equation model can be written as

$$\partial_t U + \partial_x F(U) + H(U)\partial_x \alpha_k = S(U), \tag{3.6}$$

where

$$\begin{aligned} U &= \begin{pmatrix} \alpha_1 \\ \alpha_1\rho_1 \\ \alpha_1\rho_1u_1 \\ \alpha_1\rho_1e_1 \\ (1-\alpha_1)\rho_2 \\ (1-\alpha_1)\rho_2u_2 \\ (1-\alpha_1)\rho_2e_2 \end{pmatrix}, \quad F(U) = \begin{pmatrix} 0 \\ \alpha_1\rho_1u_1 \\ \alpha_1\rho_1u_1^2 + \alpha_1p_1 \\ \alpha_1\rho_1e_1u_1 + \alpha_1p_1u_1 \\ (1-\alpha_1)\rho_2u_2 \\ (1-\alpha_1)\rho_2u_2^2 + (1-\alpha_1)p_2 \\ (1-\alpha_1)\rho_2e_2u_2 + (1-\alpha_1)p_2u_2 \end{pmatrix}, \\ H(U) &= \begin{pmatrix} u_2 \\ 0 \\ -p_1 \\ -p_1u_2 \\ 0 \\ -p_1 \\ -p_1u_2 \end{pmatrix}, \qquad S(U) = \begin{pmatrix} \Phi_1 \\ \Gamma_1 \\ \Lambda_1 \\ \Psi_1 \\ \Gamma_2 \\ \Lambda_2 \\ \Psi_2 \end{pmatrix}. \end{aligned} \tag{3.7}$$

The speed of sound c_k in phase k is defined by

$$\rho_k c_k^2 = (\partial_{p_k}\varepsilon_k)^{-1}\left(\frac{p_k}{\rho_k} - \rho_k(\partial_{\rho_k}\varepsilon_k)\right). \tag{3.8}$$

3.2 Relaxation terms

In the seven-equation model (3.1) the terms on the right hand side are called the source terms. The source terms are relaxation terms, which provide the "relaxation" on four different quantities;

u, p, g and T. Where g stands for the Gibbs-free enthalpy and the relaxation on g models the mass transfer between the liquid and the vapour. T represents the temperature and the relaxation on T models the heat transfer between the phases. The relaxation on u and p model the transfer of drag and pressure between the two different phases.

$$\begin{cases} \Phi_k & \\ \Gamma_k & \\ \Lambda_k & = D_k + \mathcal{U}\Gamma_k \\ \Psi_k & = Q_k + \mathcal{U}D_k + \mathcal{H}\Gamma_k - p_I\Phi_k \end{cases}, \tag{3.9}$$

with $\mathcal{U} = \frac{u_1+u_2}{2}$, $\mathcal{H} = \frac{u_1 u_2}{2}$ and again $p_I = p_1$. The different relaxation terms are [15]:

pressure term:

$$\Phi_k = \frac{1}{\tau_p p_{ref}} \alpha_k \alpha_j (p_k - p_j), \tag{3.10}$$

mass transfer:

$$\Gamma_k = \frac{1}{\tau_\mu \mu_{ref}} \frac{m_k m_j}{m_k + m_j} (\mu_j - \mu_k), \tag{3.11}$$

drag term:

$$D_k = \frac{1}{\tau_u} \frac{m_k m_j}{m_k + m_j} (u_j - u_k), \tag{3.12}$$

heat transfer:

$$Q_k = \frac{1}{\tau_T} \frac{m_k C_{v,k} m_j C_{v,j}}{m_k C_{v,k} + m_j C_{v,j}} (T_j - T_k), \tag{3.13}$$

with $j = 3 - k$, $\mu_k = \frac{g_k}{T_k}$ the chemical potential, $g_k = \varepsilon_k + \frac{p_k}{\rho_k} - T_k s_k$ the Gibbs enthalpy, s_k the entropy, $C_{v,k}$ the specific heat capacity, $m_k = \alpha_k \rho_k$ and $p_{ref} = |p_1| + |p_2|$ and $\mu_{ref} = |\mu_1| + |\mu_2|$. Note that for the four relaxation terms it holds that $\Phi_k = -\Phi_j$, $\Gamma_k = -\Gamma_j$, $D_k = -D_j$ and $Q_k = -Q_j$.

In the relaxation terms, time scales τ_ξ are present for the relaxation of the four different quantities: pressure, mass, temperature and the velocity between the two phases. The time scales are constant and define the rate in which the relaxation is applied.

Chapter 4

Equation of state

For the computation with the seven-equation model an equation of state is needed. The equation of state defines the relation between the internal energy, the density and the pressure. The one adopted herein is the stiffened gas equation of state, which is used for both phases.

4.1 Stiffened gas equation of state

The stiffened gas Equation Of State (EOS) [16, 17], which is given by the specific internal energy

$$\varepsilon_k = \frac{p_k + \gamma_k \pi_k}{(\gamma_k - 1)\rho_k} + q_k, \tag{4.1}$$

requires five constant parameters; the specific isochoric heat capacity $C_{v,k}$, the specific heat ratio γ_k, the reference pressure π_k, the reference energy q_k and the reference entropy q'_k for both phases. To get the ten constants, or so-called thermodynamic quantities; also the definitions for the temperature and the specific entropy are needed:

$$T_k = \frac{p_k + \pi_k}{C_{v_k}(\gamma_k - 1)\rho_k} \tag{4.2}$$

$$s_k = C_{v_k} \ln\left(\frac{p_k + \pi_k}{(C_{v_k}(\gamma_k - 1)\rho_k)^{\gamma_k}}\right) + q'_k. \tag{4.3}$$

When the coefficients are chosen as; $\pi_k = q_k = q'_k = 0$, the perfect gas EOS is retrieved. The International Association for the Properties of Water and Steam (IAPWS) [18] is an international non-profit association that provides internationally accepted properties of water and steam. In the official water and steam tables of the IAPWS the thermodynamic properties of water and steam are presented. To get all ten parameters for experiments these tables and the equations for the thermodynamic quantities are used.

4.2 Estimation of the coefficients

The stiffened gas EOS gives an estimation of the ten thermodynamic coefficients, which are material properties. The values can be estimated from the water and steam tables. Around the reference temperature T_{ref}, which is chosen according to the initial temperature in the experiment, the approximation of the coefficients should lead to values for ε_k, T_k and s_k close to these from the tables.

In the technical report of E. Blaud et al. [17], based on Le Métayer et al. [16], the calculations to generate the thermodynamic coefficients ($C_{v,k}$, γ_k, π_k, q_k and q'_k) from the values of the water and steam tables are given. For the calculation of the specific heat capacity $C_{p,k}$ for phase k, a temperature interval $[T_1, T_2]$ is chosen to linearly approximate the slope of the enthalpy over

the temperature derived from $h_k(T) = C_{p,k}T + q_k(T_{ref})$, here $q_k(T_{ref})$ is the value of reference energy of the stiffened gas EOS at reference temperature T_{ref}, which are retrieved from the steam and water tables. And thus the specific heat capacity is calculated as

$$C_{p,k} = \frac{h_k(T_2) - h_k(T_1)}{T_2 - T_1}. \tag{4.4}$$

In Figure 4.1 it can be seen that for high temperatures the slope of the enthalpy-temperature curve of vapour is negative, which means that a negative value for $C_{p,v}$, the specific heat capacity is obtained and this is physically not feasible. This means that for this temperature range the estimation of $C_{p,k}$ in (4.4) retrieves no useful. So in case of a high reference temperatures a temperature interval is chosen which does not contain the reference temperature T_{ref}.

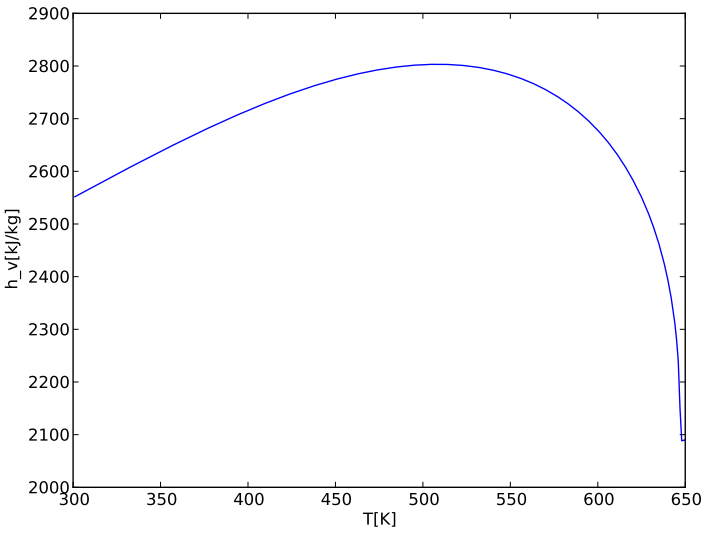

Figure 4.1: Curve of the enthalpy of water vapour over the temperature at the saturation pressure, retrieved from the water and steam tables.

To avoid the choice of the temperature interval and the negative value for the specific heat capacity, it is proposed to use the value for $C_{p,k}$ from the water and steam tables at the chosen reference temperature. The constants can then be calculated using the stiffened gas equation of state (4.1), the equations for the temperature (4.2), the specific entropy (4.3) and the equation for the celerity. For the stiffened gas EOS, the equation for the celerity is given by

$$\begin{aligned} c_k^2 &= \gamma_k \frac{p_k + \pi_k}{\rho_k} \\ &= \gamma_k C_{v,k}(\gamma_k - 1)T_k. \end{aligned} \tag{4.5}$$

Now the constants are calculated using the following procedure:

$$C_{v,k} = \frac{T_{ref} {C_{p,k}}^2}{{c_k}^2 + C_{p,k} T_{ref}} \tag{4.6}$$

$$\gamma_k = \frac{C_{p,k}}{C_{v,k}} \tag{4.7}$$

$$\pi_k = \rho_k(\gamma_k - 1) C_{v,k} T_{ref} - p_{sat} \tag{4.8}$$

$$q_k = h_k - C_{p,k} T_{ref} \tag{4.9}$$

$$g_k = h_k - T_{ref} s_k \tag{4.10}$$

$$q'_k = \gamma_k C_{v,k} - \frac{g_k}{T_{ref}} - C_{v,k} \ln\left(\frac{T_{ref}^{\gamma_k}}{(p_{sat} + \pi_k)^{\gamma_k - 1}}\right) + \frac{q_k}{T_{ref}}. \tag{4.11}$$

Here the green coloured values ξ are retrieved from the water and steam tables, at the reference temperature T_{ref} and the associated saturation pressure $p_{sat}(T_{ref})$.

This new estimation, based on the chosen reference temperature T_{ref}, of the stiffened gas equation of state coefficients is implemented in a python code that uses the IAPWS (1997) official tables with the properties of water and steam, to easily get the values for the coefficients for all experiments.

This new approximation gives the required thermodynamic coefficients for the experiments simulated in Chapter 6.

4.3 Comparison with the IAPWS water and steam tables

For the validation of the new "calibration" of the stiffened gas EOS coefficients the results of the approximation are compared with the values in the IAPWS tables. To retrieve good results in simulations where cavitation or condensation occurs, an important requirement is that the approximation of the saturation curve is close to the one from the table. Furthermore the results on the celerity and the specific enthalpy are compared with the values from the tables.

To find the saturation curve from the "calibrated" coefficients the equation for the Gibbs free energy is used;

$$g_k = (\gamma_k C_{v,k} - q'_k)\, T - C_{v,k} T \ln\left(\frac{T^{\gamma_k}}{(p_k + \pi_k)^{\gamma_k - 1}}\right) + q_k. \tag{4.12}$$

At the saturation curve the Gibbs free energy of the liquid is equal to the Gibbs free energy of the vapour, therefore the bisection method is used to find $p_{sat}(T)$, such that

$$g_1(p_{sat}(T), T) = g_2(p_{sat}(T), T). \tag{4.13}$$

The saturation curve calculated with the new calibration at $T_{ref} = 300$ K, $T_{ref} = 355$ K and $T_{ref} = 515$ K are shown in Figure 4.2. These temperatures are the initial temperatures in the experiments in Chapter 6. With the new calibration a similar saturation curve is retrieved, for all reference temperatures. At the reference temperature the value of the approximated saturation pressure is exactly equal to the value from the table and around this temperature a small error is visible.

To retrieve the curve of the enthalpy using the coefficients, the equation

$$h_k(T) = \gamma_k C_{v,k} T + q_k \tag{4.14}$$

is used. And to approximate the curve of the speed of sound,

$$c_k(T) = \sqrt{\gamma_k C_{v,k}(\gamma_k - 1)T} \tag{4.15}$$

is used where $\gamma_k, C_{v,k}$ and q_k are the new calibrated coefficients. The enthalpy curves and the speed of sound curves using reference temperatures $T_{ref} = 300$ K, $T_{ref} = 355$ K and $T_{ref} = 515$ K are compared with the values from the water and steam tables and shown in Figures 4.3 - 4.5.

In the figures it can be seen that at the reference temperature the approximation is exactly equal to the value from the table for the entropy and the speed of sound. For the values around the reference temperature some deviations can be observed. For a low reference temperature the curves lie close to the curves from the table.

To further validate the new approximation of the coefficients they are used in the simulations of the seven-equation model in this report.

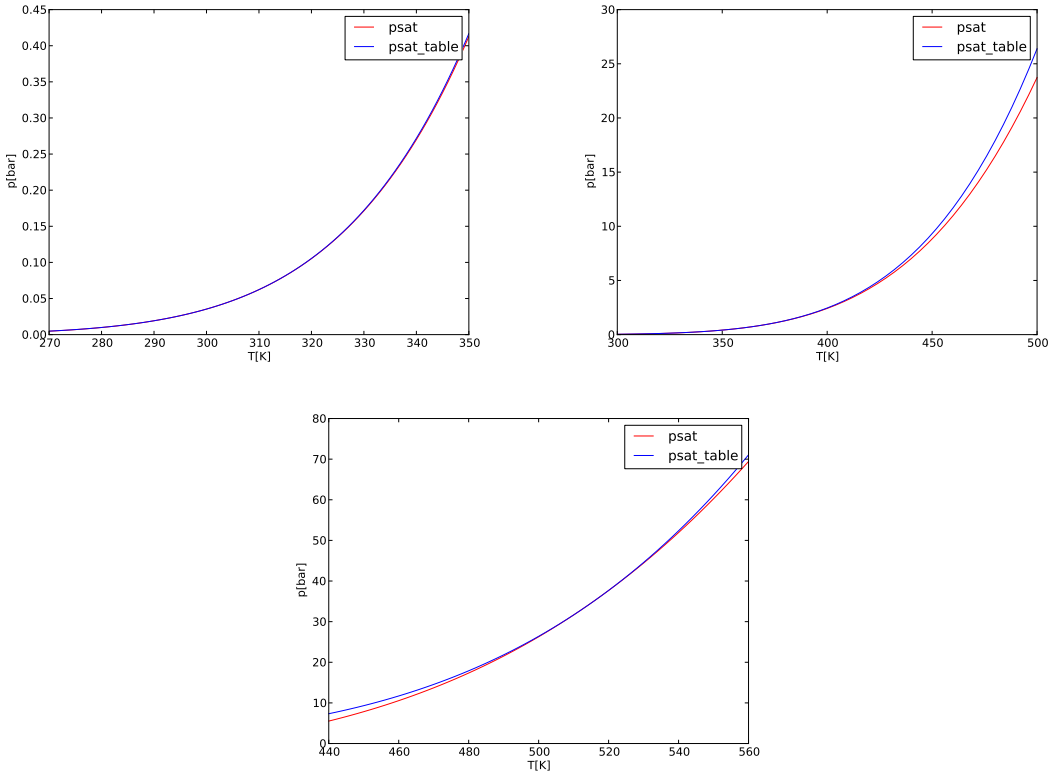

Figure 4.2: Boiling temperatures as function of pressure, retrieved from the water and steam tables (blue line) and the new calibration of the coefficients (red line). Left is approximated with reference temperature $T_{ref} = 300$ K, right for $T_{ref} = 355$ K and below for $T_{ref} = 515$ K.

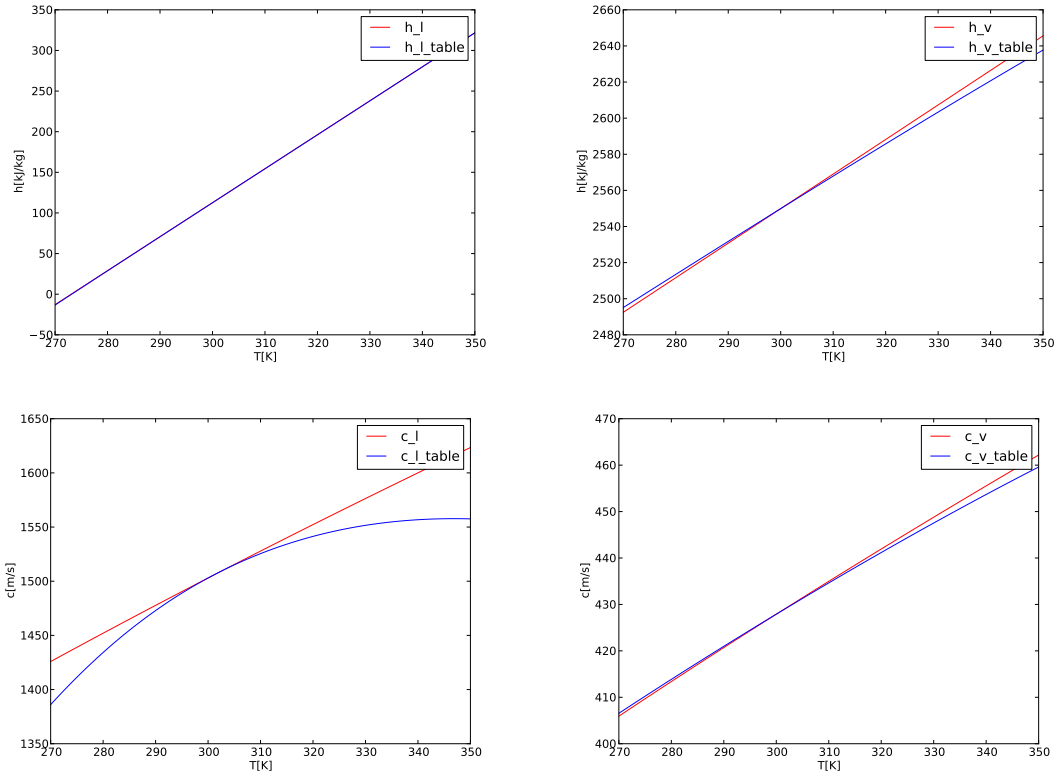

Figure 4.3: Results using $T_{ref} = 300$ K. Above the curves of the enthalpy are shown, left for the liquid phase right for the vapour phase. Below the curves for the speed of sound are shown, left for the liquid phase right for the vapour phase.

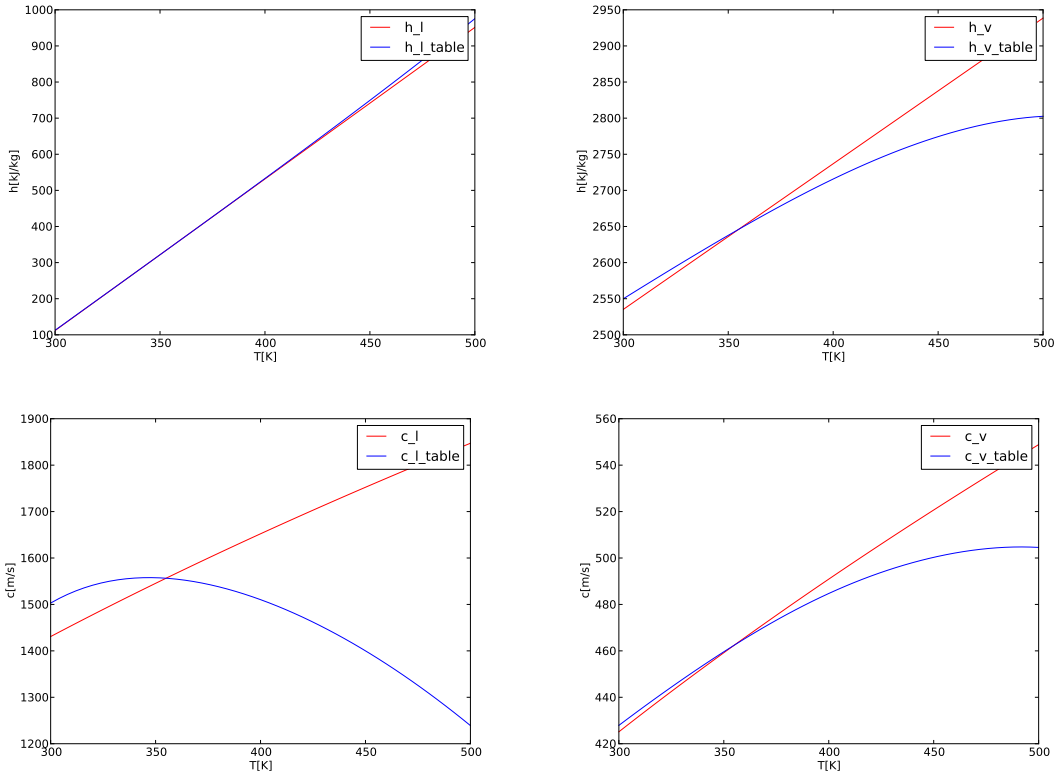

Figure 4.4: Results using $T_{ref} = 355$ K. Above the curves of the enthalpy are shown, left for the liquid phase right for the vapour phase. Below the curves for the speed of sound are shown, left for the liquid phase right for the vapour phase.

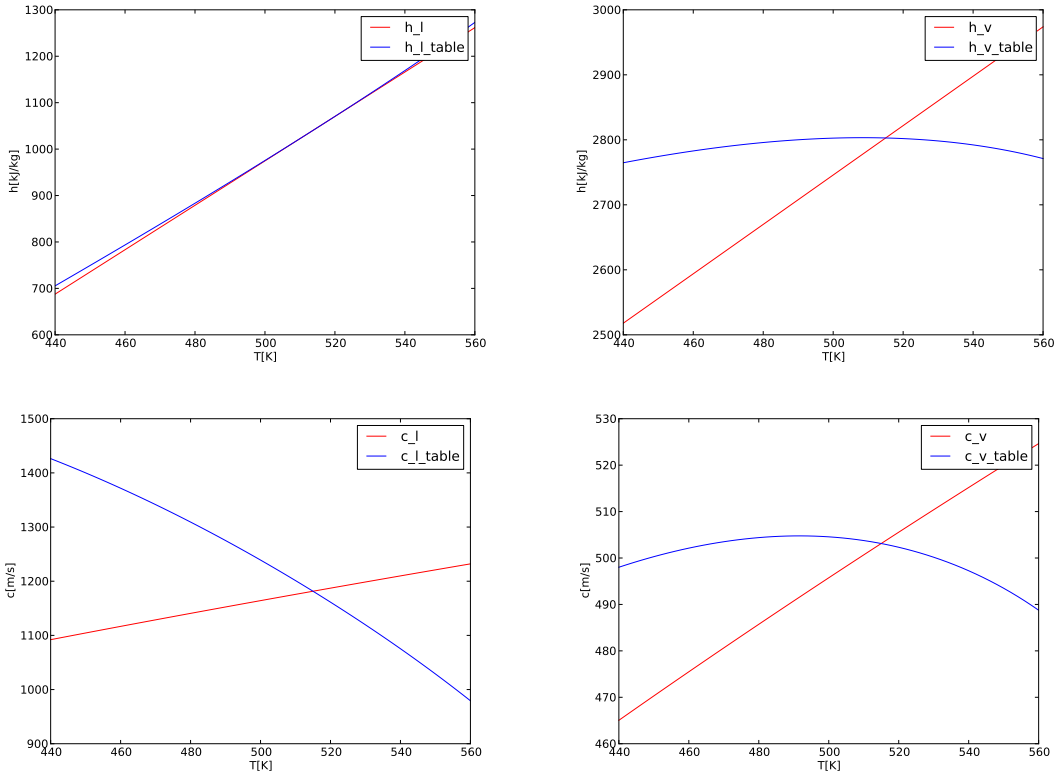

Figure 4.5: Results using $T_{ref} = 515$ K. Above the curves of the enthalpy are shown, left for the liquid phase right for the vapour phase. Below the curves for the speed of sound are shown, left for the liquid phase right for the vapour phase.

4.4 Adjustments to simulate pipe wall elasticity

Further on in the calculations done with the seven-equation model the thermodynamic coefficients are adjusted to account for the elasticity of the pipe. This is done approximating the coefficients using a lowered speed of sound in the liquid c_l. In the new calibration of the coefficients the adjustment can be made easily by choosing a fixed value for the celerity c_l instead of retrieving the value from the water and steam tables.

Results using this adjusted celerity are presented in Chapter 6.3, in the cold water hammer test facility experiment.

Chapter 5

Numerical methods

For the computation of the seven-equation model, the fractional step method [15] is used. This method consists of two steps to retrieve the values of ρ_k, p_k, u_k and α_k in the system. The first step of this method is the convection step, where the homogeneous system, which is the seven-equation model (3.6) without the source terms,

$$\partial_t U + \partial_x F(U) + H(U)\partial_x \alpha_K = 0, \tag{5.1}$$

is solved numerically. The numerical approximation is done using a finite volume method to get the discretized form. After the convection step the relaxation step, $\partial_t U = S(U)$, is applied. Note that the terms of $S(U)$ are constructed by different relaxation terms given in Equation (3.10) - (3.13). Therefore the relaxation step is split into four substeps, one for the relaxation of each quantity. So using the convection step on the initial values φ^n the updated value $\tilde{\varphi}$ is retrieved. After this step the different relaxation steps are applied and from $\tilde{\varphi}$ the updated value φ^{n+1} is retrieved.

$$\varphi^n \xrightarrow{\text{convection step}} \tilde{\varphi} \xrightarrow{\text{relaxation step}} \varphi^{n+1}$$
$$\xleftarrow{\qquad\qquad\qquad\qquad\qquad\qquad} .$$

5.1 Convection step

A finite volume method is used for the convection part of the system (5.1); therefore the computational domain is split into intervals, $[x_{i-1/2}, x_{i+1/2}]$ with width Δx_i and the time steps are chosen $[t^n, t^{n+1}]$ with a length of Δt^n. The size of the time step is retrieved from the Courant-Friedrichs-Lewy (CFL) condition. The CFL condition is necessary for the stability of the system, it is given by $\mathcal{C} = \lambda \frac{\Delta t}{\Delta x}$, where λ is the highest wave speed and $\mathcal{C}$ the Courant number which lies between 0 and 1. The integral form of the homogeneous part of the model is given by

$$\begin{aligned} 0 &= \int_{t^n}^{t^{n+1}} \int_{x_{i-1/2}}^{x_{i+1/2}} \left(\partial_t U + \partial_x F(U) + H(U)\partial_x \alpha_k\right) \mathrm{d}x\mathrm{d}t \\ &= \int_{t^n}^{t^{n+1}} \int_{x_{i-1/2}}^{x_{i+1/2}} \partial_t U \ \mathrm{d}x\mathrm{d}t + \int_{t^n}^{t^{n+1}} \int_{x_{i-1/2}}^{x_{i+1/2}} \partial_x F(U) \ \mathrm{d}x\mathrm{d}t \\ &\quad + \int_{t^n}^{t^{n+1}} \int_{x_{i-1/2}}^{x_{i+1/2}} H(U)\partial_x \alpha_k \ \mathrm{d}x\mathrm{d}t. \end{aligned} \tag{5.2}$$

Now the integrals are numerically approximated, this gives the equation

$$0 \approx \Delta x_i \left[U_i^{n+1} - U_i^n\right] + \Delta t^n \left[F_{i+1/2} - F_{i-1/2}\right] + \Delta t^n \left[H_{i+1/2}^- - H_{i-1/2}^+\right], \tag{5.3}$$

for

$$U_i^n \approx \frac{1}{\Delta x_i} \int_{x_{i-1/2}}^{x_{i+1/2}} U(x,t^n)\mathrm{d}x \tag{5.4}$$

$$F_{i+1/2} \approx \frac{1}{\Delta t^n} \int_{t^n}^{t^{n+1}} F(U(x_{i+1/2},t))\mathrm{d}t \tag{5.5}$$

$$H_{i+1/2}^- - H_{i-1/2}^+ \approx \frac{1}{\Delta t^n} \int_{t^n}^{t^{n+1}} \int_{x_{i-1/2}}^{x_{i+1/2}} H(U(x,t))\partial_x \alpha_k \ \mathrm{d}x\mathrm{d}t. \tag{5.6}$$

For the numerical approximation of the integrals several numerical schemes can be used. The ones that are implemented in the Europlexus code for the seven-equation model [19] are the Rusanov, the HLL and the HLLC [20, 21] schemes. For the validation of the seven-equation model the Rusanov and the HLLC schemes are used.

5.1.1 Rusanov scheme

The non-conservative first-order Rusanov scheme is given for the seven-equation model by

$$F_{i+1/2}^{Rus}(U_i^n, U_{i+1}^n) = \frac{1}{2}\left[F(U_i^n) + F(U_{i+1}^n) - r_{i+1/2}(U_{i+1}^n - U_i^n)\right], \tag{5.7}$$

with $r_{i+1/2}$ the maximum of the spectral radius of the convection matrix.

$$r_{i+1/2} = \max\left(|(u_1)_m^n| + (c_1)_m^n, |(u_2)_m^n| + (c_2)_m^n\right), \text{ for } m = i, i+1. \tag{5.8}$$

And

$$H_{i+1/2}^- - H_{i-1/2}^+ = H(U_i^n)\left[(\alpha_k)_{i+1/2} - (\alpha_k)_{i-1/2}\right], \tag{5.9}$$

where the numerical value $(\alpha_k)_{i+1/2}$ is given by

$$(\alpha_k)_{i+1/2} = \frac{1}{2}\left[(\alpha_k)_i + (\alpha_k)_{i+1}\right]. \tag{5.10}$$

5.1.2 HLLC scheme

The HLLC scheme proposed by S.A. Tokareva and E.F. Toro [20] for the seven-equation Baer-Nunziato model is more complex than the Rusanov scheme, but more accurate. The HLLC scheme is a complete approximate Riemann solver as all the characteristic fields present in the exact solution of the Riemann problem are taken into account in the construction of the numerical fluxes. So all six different wave speeds, $u_k - c_k, u_k, u_k + c_k$, for k equal to 1 or 2, are incorporated in the approximation of the flux. In Figure 5.1 all the waves are shown with the different characteristic fields for $(S_2)_M < (S_1)_M$, where $(S_k)_L$ represents the wave with speed $u_k - c_k$, $(S_k)_M$ the wave with speed u_k and $(S_k)_R$ the wave with wave speed $u_k + c_k$.

The numerical treatment of the genuinely nonlinear waves $(S_k)_K$ with $k = 1, 2$ and $K = L, R$, as there is no jump of the volume fraction, is based on averaged Rankine-Hugoniot type relations. This is done classically with the HLLC scheme for the Euler equations. Then, the preservation of the Riemann invariants is used for the linear degenerate waves $(S_k)_M$ with $k = 1, 2$. Finally, this leads to a nonlinear system of four equations connecting the unknowns to the initial conditions left and right of the interface, which is solved using an iterative Newton-Raphson approach. By the Baer-Nunziato choice of $u_I = u_2$, the integrals of the non-conservative terms are only active across the contact of phase 2, and is estimated using the thin-layer approximation proposed by Schwendeman et al. [22]. This approximation is based on the regularization of the solution across $(S_2)_M$, which is replaced by a thin-layer. More information on this can be found in [20, 21].

So in the case where $(S_2)_M < (S_1)_M$, the values of the first-order HLLC flux are given for phase 1 by

$$F_{i+1/2}^{HLLC} = \begin{cases} F_{1,L} = F(U_{1,L}) & \text{if } 0 < (S_1)_L \\ F_{1,L}^* = F_{1,L} + (S_1)_L \left(U_{1,L}^* - U_{1,L}\right) & \text{if } (S_1)_L \leq 0 < (S_2)_M \\ F_{1,M}^* = F_{1,R}^* + (S_1)_M \left(U_{1,M}^* - U_{1,R}^*\right) & \text{if } (S_2)_M \leq 0 < (S_1)_M \\ F_{1,R}^* = F_{1,R} + (S_1)_R \left(U_{1,R}^* - U_{1,R}\right) & \text{if } (S_1)_M \leq 0 < (S_1)_R \\ F_{1,R} = F(U_{1,R}) & \text{if } (S_1)_R \leq 0 \end{cases}, \tag{5.11}$$

and for phase 2 by

$$F_{i+1/2}^{HLLC} = \begin{cases} F_{2,L} = F(U_{2,L}) & \text{if } 0 < (S_2)_L \\ F_{2,L}^* = F_{2,L} + (S_2)_L \left(U_{2,L}^* - U_{2,L}\right) & \text{if } (S_2)_L \leq 0 < (S_2)_M \\ F_{2,R}^* = F_{2,R} + (S_2)_R \left(U_{2,R}^* - U_{2,R}\right) & \text{if } (S_2)_M \leq 0 < (S_2)_R \\ F_{2,R} = F(U_{2,R}) & \text{if } (S_2)_R \leq 0 \end{cases}. \tag{5.12}$$

The values for $H_{i+1/2}^-$ and $H_{i-1/2}^+$ are calculated using the thin-layer approximation.

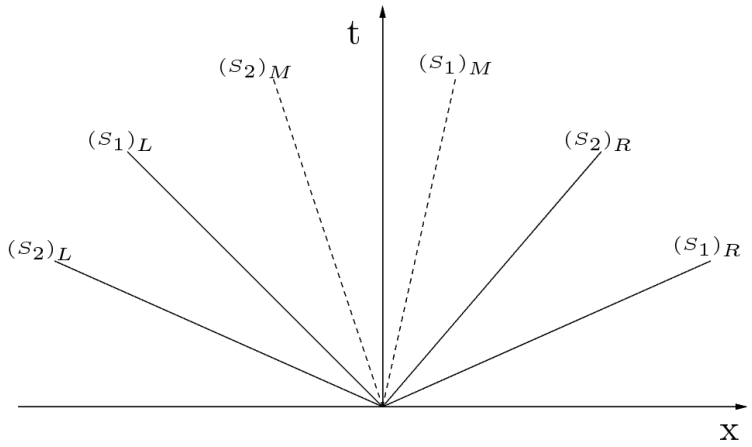

Figure 5.1: Waves present in the seven-equation model in the x, t plane.

So in the convection step at time interval $[t^n, t^{n+1}]$, with the given initial value φ^n, the approximate solution is computed, $\tilde{\varphi}$. Then this solution $\tilde{\varphi}$ is provided as the initial values for the relaxation step.

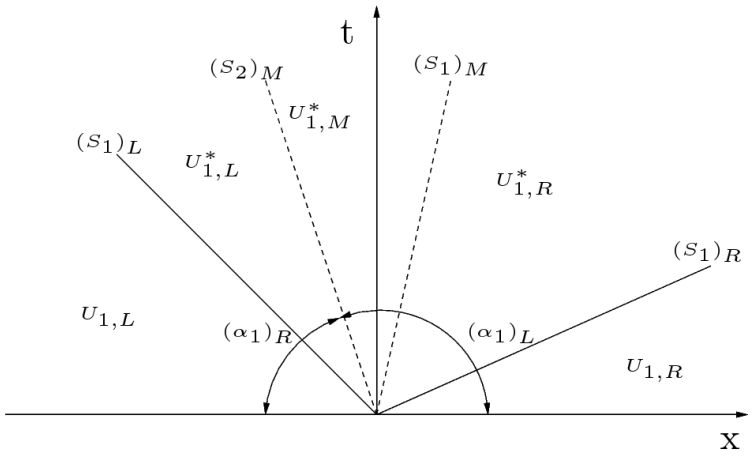

Figure 5.2: States for the different characteristic fields for phase 1.

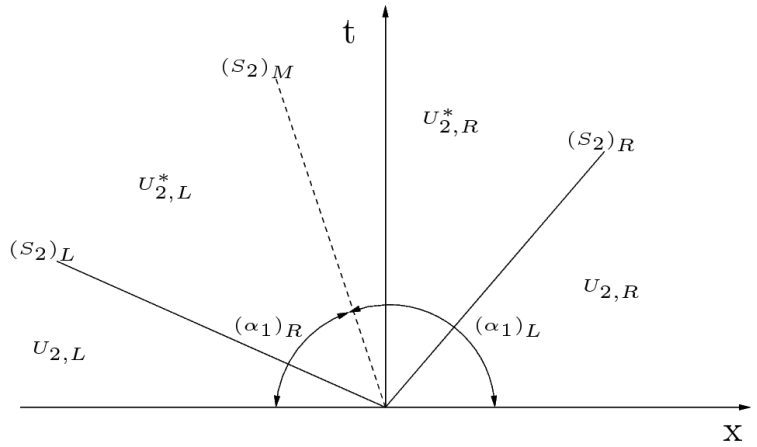

Figure 5.3: States for the different characteristic fields for phase 2.

5.2 Relaxation step

The relaxation step is divided into four substeps, one substep for the relaxation of each quantity; p, u, T and g, see also (3.10) - (3.13). In the relaxation steps the notation φ^0 is used for the value of φ retrieved at the end of the previous substep. The notation φ^* is used as the value of φ at the end of the relaxation substep. Furthermore $m_k = \alpha_k \rho_k$, is the partial mass of phase k and the length of the time step Δt is used. Recall from Section 3.2 that the relaxation therms are

$$\Phi_k = \frac{1}{\tau_p p_{ref}} \alpha_k \alpha_j (p_k - p_j) \tag{5.13}$$

$$D_k = \frac{1}{\tau_u} \frac{m_k m_j}{m_k + m_j} (u_j - u_k) \tag{5.14}$$

$$Q_k = \frac{1}{\tau_T} \frac{m_k C_{v,k} m_j C_{v,j}}{m_k C_{v,k} + m_j C_{v,j}} (T_j - T_k) \tag{5.15}$$

$$\Gamma_k = \frac{1}{\tau_\mu \mu_{ref}} \frac{m_k m_j}{m_k + m_j} (\mu_j - \mu_k), \tag{5.16}$$

with $j = 3 - k$.

5.2.1 Pressure relaxation

The system that is approximated for the pressure relaxation for the two different phases is

$$\begin{cases} \partial_t \alpha_k & = \Phi_k \\ \partial_t(\alpha_k \rho_k) & = 0 \\ \partial_t(\alpha_k \rho_k u_k) & = 0 \\ \partial_t(\alpha_k \rho_k e_k) & = -p_I \Phi_k \end{cases}. \tag{5.17}$$

The values for m_k and u_k are taken constant over time, so $m_k^* = m_k^0$ and $u_k^* = u_k^0$. The following implicit scheme is used to update the value α_k :

$$\frac{\alpha_k^* - \alpha_k^0}{\Delta t} = \frac{1}{\tau_p p_{ref}} \alpha_k^* \alpha_j^* (p_k^* - p_j^*). \tag{5.18}$$

An iterative procedure is used to compute α_k^* and the pressure p_k^* from the results of the previous step. Then e_k is obtained using:

$$\frac{m_k^* e_k^* - m_k^0 e_k^0}{\Delta t} = -p_I^* \frac{\alpha_k^* - \alpha_k^0}{\Delta t}. \tag{5.19}$$

5.2.2 Velocity relaxation

The system that is approximated for the velocity relaxation for the two different phases is

$$\begin{cases} \partial_t \alpha_k & = 0 \\ \partial_t(\alpha_k \rho_k) & = 0 \\ \partial_t(\alpha_k \rho_k u_k) & = D_k \\ \partial_t(\alpha_k \rho_k e_k) & = \mathcal{U} D_k \end{cases}. \tag{5.20}$$

The values for α_k and m_k are assumed not to change over time, so $\alpha_k^* = \alpha_k^0$ and $m_k^* = m_k^0$. Furthermore from the second and third equation of (5.20),

$$D_k = \partial_t(m_k u_k) = m_k \partial_t u_k \tag{5.21}$$

so that

$$\begin{aligned} \partial_t(u_k - u_j) &= \frac{D_k}{m_k} - \frac{D_j}{m_j} \\ &= \frac{1}{\tau_u} \frac{m_j}{m_k + m_j}(u_j - u_k) - \frac{1}{\tau_u} \frac{m_k}{m_k + m_j}(u_k - u_j) \\ &= -\frac{1}{\tau_u}(u_k - u_j). \end{aligned} \tag{5.22}$$

Now introduce $u_d = (u_1 - u_2)$, with $\partial_t u_d = -\frac{1}{\tau_u} u_d$, where u_1 is the velocity of phase 1 and u_2 is the velocity of phase 2. This means that u_d is of the form $u_d = Ce^{-t/\tau_u}$, where C is a constant with respect to time. Note that $D_k = -D_j$, then

$$\begin{aligned} u_1 &= \frac{m_1 u_1 + m_2 u_2 + m_2 u_d}{m_1 + m_2} \\ &= \frac{m_1 u_1 + m_2 u_2}{m_1 + m_2} + \frac{m_2}{m_1 + m_2} u_d \\ \partial_t u_1 &= \frac{1}{m_1 + m_2} \partial_t(m_1 u_1 + m_2 u_2) + \frac{m_2}{m_1 + m_2} \partial_t u_d \\ &= \frac{1}{m_1 + m_2}(D_1 + D_2) + \frac{m_2}{m_1 + m_2} \partial_t u_d \\ &= \frac{m_2}{m_1 + m_2} \partial_t u_d. \end{aligned} \tag{5.23}$$

In a discretized form this is;

$$\begin{aligned}\frac{u_1^* - u_1^0}{\Delta t} &= \frac{m_2^0}{m_1^0 + m_2^0}\frac{u_d^* - u_d^0}{\Delta t} \\ &= \frac{m_2^0}{m_1^0 + m_2^0}\frac{u_d^0(e^{-\Delta t/\tau_u} - 1)}{\Delta t},\end{aligned} \tag{5.24}$$

and thus the updated values are given by

$$u_1^* = u_1^0 + \frac{m_2^0}{m_1^0 + m_2^0}\left(e^{-\Delta t/\tau_u} - 1\right)(u_1^0 - u_2^0). \tag{5.25}$$

The same calculations and discretization can be done for u_2, hence

$$u_2^* = u_2^0 + \frac{m_1^0}{m_1^0 + m_2^0}\left(e^{-\Delta t/\tau_u} - 1\right)(u_2^0 - u_1^0). \tag{5.26}$$

For the specific internal energy the same derivation can be done. Note that the total specific energy is $e_k = \varepsilon_k + \frac{1}{2}u_k^2$, so that

$$\begin{aligned}\partial_t(m_k e_k) &= m_k \partial_t e_k \\ &= m_k \partial \varepsilon_k + m_k u_k \partial_t u_k \\ &= \frac{u_j + u_k}{2} D_k \\ \partial_t \varepsilon_k &= -u_k \partial_t u_k + \frac{1}{m_k}\frac{u_j + u_k}{2} D_k \\ &= -u_k \partial_t u_k + \frac{u_j + u_k}{2}\partial_t u_k \\ &= \frac{u_j - u_k}{2}\partial_t u_k.\end{aligned} \tag{5.27}$$

Now use the calculations (5.23) and discretization (5.24) and find

$$\begin{aligned}\partial_t \varepsilon_1 &= \frac{u_2 - u_1}{2}\partial_t u_1 \\ &= -\frac{u_d}{2}\frac{m_2}{m_1 + m_2}\partial_t u_d \\ &= -\frac{1}{2}\frac{m_2}{m_1 + m_2}\partial_t(\frac{1}{2}u_d^2),\end{aligned} \tag{5.28}$$

with discretized form

$$\begin{aligned}\frac{\varepsilon_1^* - \varepsilon_1^0}{\Delta t} &= -\frac{1}{4}\frac{m_2^0}{m_1^0 + m_2^0}\frac{(u_d^*)^2 - (u_d^0)^2}{\Delta t} \\ &= -\frac{1}{4}\frac{m_2^0}{m_1^0 + m_2^0}\frac{(u_d^0)^2(e^{-2\Delta t/\tau_t} - 1)}{\Delta t},\end{aligned} \tag{5.29}$$

and thus the updated values are retrieved by

$$\varepsilon_1^* = \varepsilon_1^0 + \frac{1}{4}\frac{m_2^0}{m_1^0 + m_2^0}\left(1 - e^{-2\Delta t/\tau_u}\right)(u_2^0 - u_1^0)^2. \tag{5.30}$$

Again the same can be done for ε_2, leading to

$$\varepsilon_2^* = \varepsilon_2^0 + \frac{1}{4}\frac{m_1^0}{m_1^0 + m_2^0}\left(1 - e^{-2\Delta t/\tau_u}\right)(u_1^0 - u_2^0)^2. \tag{5.31}$$

5.2.3 Temperature relaxation

For the relaxation of the temperature the following system is approximated for the two different phases

$$\begin{cases} \partial_t \alpha_k & = 0 \\ \partial_t(\alpha_k \rho_k) & = 0 \\ \partial_t(\alpha_k \rho_k u_k) & = 0 \\ \partial_t(\alpha_k \rho_k e_k) & = Q_k \end{cases}. \tag{5.32}$$

The values for α_k, m_k and u_k are not allowed to change within the duration Δt of the time interval, so $\alpha_k^* = \alpha_k^0$, $m_k^* = m_k^0$ and $u_k^* = u_k^0$. Furthermore, note that $\varepsilon_k = C_{v,k} T_k + q_k$, where q_k and $C_{v,k}$ are constants, so that $e_k = C_{v,k} T_k + q_k + \frac{1}{2} u_k^2$. Now derive

$$Q_k = \partial_t(m_k e_k) = m_k \partial_t e_k, \tag{5.33}$$

so that for the temperature T_1 of phase 1 and the temperature T_2 of phase 2

$$\begin{aligned} \partial_t(T_1 - T_2) &= \frac{1}{C_{v,1}} \partial_t e_1 - \frac{1}{C_{v,2}} \partial_t e_2 \\ &= \frac{Q_1}{m_1 C_{v,1}} - \frac{Q_2}{m_2 C_{v,2}} \\ &= \frac{1}{\tau_T} \frac{m_2 C_{v,2}}{m_1 C_{v,1} + m_2 C_{v,2}} (T_2 - T_1) - \frac{1}{\tau_T} \frac{m_1 C_{v,1}}{m_1 C_{v,1} + m_2 C_{v,2}} (T_1 - T_2) \\ &= -\frac{1}{\tau_T} (T_1 - T_2). \end{aligned} \tag{5.34}$$

The value $T_d = (T_1 - T_2)$ is introduced, with $\partial_t T_d = -\frac{1}{\tau_T} T_d$. This means that T_d is of the form $T_d = C e^{-t/\tau_T}$, where C is a constant with respect to time. Note that $Q_k = -Q_j$, so then similar calculations as in (5.23) are done to arrive at

$$\begin{aligned} T_1 &= \frac{m_1 C_{v,1} T_1 + m_2 C_{v,2} T_2 + m_2 C_{v,2} T_d}{m_1 C_{v,1} + m_2 C_{v,2}} \\ &= \frac{m_1 C_{v,1} T_1 + m_2 C_{v,2} T_2}{m_1 C_{v,1} + m_2 C_{v,2}} + \frac{m_2 C_{v,2}}{m_1 C_{v,1} + m_2 C_{v,2}} T_d \\ \partial_t T_1 &= \frac{m_1 \partial_t(C_{v,1} T_1) + m_2 \partial_t(C_{v,2} T_2)}{m_1 C_{v,1} + m_2 C_{v,2}} + \frac{m_2 C_{v,2}}{m_1 C_{v,1} + m_2 C_{v,2}} \partial_t T_d \\ &= \frac{Q_1 + Q_2}{m_1 C_{v,1} + m_2 C_{v,2}} + \frac{m_2 C_{v,2}}{m_1 C_{v,1} + m_2 C_{v,2}} \partial_t T_d \\ &= \frac{m_2 C_{v,2}}{m_1 C_{v,1} + m_2 C_{v,2}} \partial_t T_d. \end{aligned} \tag{5.35}$$

In discretized form this gives

$$\begin{aligned} \frac{T_1^* - T_1^0}{\Delta t} &= \frac{m_2^0 C_{v,2}^0}{m_1^0 C_{v,1}^0 + m_2^0 C_{v,2}^0} \frac{T_d^* - T_d^0}{\Delta t} \\ &= \frac{m_2^0 C_{v,2}^0}{m_1^0 C_{v,1}^0 + m_2^0 C_{v,2}^0} \frac{T_d^0 (e^{-\Delta t/\tau_T} - 1)}{\Delta t}, \end{aligned} \tag{5.36}$$

and thus the updated value for the temperature is

$$T_1^* = T_1^0 + \frac{m_2^0 C_{v,2}^0}{m_1^0 C_{v,1}^0 + m_2^0 C_{v,2}^0} \left(e^{-\Delta t/\tau_T} - 1 \right) (T_1^0 - T_2^0). \tag{5.37}$$

The same derivation can be done for T_2, hence

$$T_2^* = T_2^0 + \frac{m_1^0 C_{v,1}^0}{m_1^0 C_{v,1}^0 + m_2^0 C_{v,2}^0} \left(e^{-\Delta t/\tau_T} - 1 \right) (T_2^0 - T_1^0). \tag{5.38}$$

5.2.4 Chemical potential relaxation

For the chemical potential relaxation, or so called mass transfer, the following system is approximated for the two different phases

$$\begin{cases} \partial_t \alpha_k & = 0 \\ \partial_t(\alpha_k \rho_k) & = \Gamma_k \\ \partial_t(\alpha_k \rho_k u_k) & = \mathcal{U}\Gamma_k \\ \partial_t(\alpha_k \rho_k e_k) & = \mathcal{H}\Gamma_k \end{cases}. \tag{5.39}$$

To simplify the calculations the system can be rewritten as

$$\begin{cases} \partial_t \alpha_k & = 0 \\ \partial_t(m_k) & = \Gamma_k \\ \partial_t(m_k u_k) & = \mathcal{U}\Gamma_k \\ \partial_t(m_k \varepsilon_k) & = 0 \end{cases}. \tag{5.40}$$

The values for α_k and $m_k\varepsilon_k$ are assumed not to change over time, so $\alpha_k^* = \alpha_k^0$ and $m_k^*\varepsilon_k^* = m_k^0\varepsilon_k^0$. The following implicit scheme is used to approximate the value m_k:

$$\frac{m_k^* - m_k^0}{\Delta t} = \frac{1}{\tau_\mu \mu_{ref}} \frac{m_k^* m_j^*}{m_k^* + m_j^*}(\mu_k^* - \mu_j^*). \tag{5.41}$$

Just as for the pressure relaxation an iterative procedure is used to approximate m_k^*. And for $m_k u_k$,

$$\frac{m_k^* u_k^* - m_k^0 u_k^0}{\Delta t} = \frac{u_k^* + u_j^*}{2} \frac{m_k^* - m_k^0}{\Delta t}, \tag{5.42}$$

again an iterative procedure is used to approximate $m_k^* u_k^*$.

Finally with the initial value φ^n, the value φ^{n+1} is determined by applying first the convection step and then the four relaxation steps.

Chapter 6

Assessment of the seven-equation model

The goal of the model is to simulate two-phase flows, such that EDF can use it to investigate the water hammers that occur in the EDF facilities. These facilities already exist, but there are no sensors to measure the location and the force of the water hammers. So the simulations done with the seven-equation model in Europlexus cannot be tested on measurements in the actual system. Therefore the seven-equation model, its relaxation terms and the new calibration of the coefficients of the stiffened gas equation of state are verified using some already known experiments. The results of the calculations done in Europlexus with the seven-equation model are compared with results from physical experiments and results from other verified models. Three different situations are modelled: the water cavitation tube problem, the Edwards pipe experiment and the cold water hammer test facility. The experiments and the results are detailed in the next paragraphs. For most calculations with the seven-equation model the Rusanov scheme is used instead of the less diffusive HLLC scheme. This has been done because in more complex simulations the HLLC scheme was not robust enough for the computations.

6.1 Water cavitation tube problem

To examine the effects of the different relaxation terms in the seven-equation, Baer-Nunziato model [11, 14] in Europlexus, the water cavitation tube problem, initially proposed in [23], is considered. The HLLC scheme is used for the discretization of the homogeneous part of the seven-equation model, i.e. the part without source terms. The Europlexus results are compared with the results of the simulations done by M. Pelanti and K.-M. Shyue [24]. They used a two-fluid, six-equation model and assume that the two phases have the same velocity u.

The water cavitation tube problem is a one-dimensional tube model containing liquid water; the model is shown in Figure 6.1. The tube is 1 m long and split into two parts of equal length, a left and right part. At $t = 0$ the velocity in the left part is $u_L = -2$ m/s and in the right part $u_R = 2$ m/s, the initial temperature is $T = 354.7$ K and the initial pressure is 1 bar absolute. In the continuation of this report the pressure will be denoted in absolute pressure. When the numerical test starts two rarefaction waves appear, travelling in opposite directions from the middle of the pipe, due to opposite signs of the initial velocities. Because of the rarefaction waves the pressure drops to saturation pressure and the liquid starts to cavitate and more vapour appears.

The initial conditions and the thermodynamic coefficients for the simulation are shown in Table 6.1 and Table 6.2. The pipe is split into 5000 cells, and for the calculations the Courant number $\mathcal{C} = 0.5$ is used. Furthermore the stiffened gas equation of state is used for both states, the liquid and the vapour.

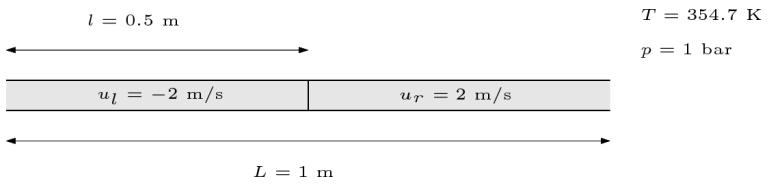

Figure 6.1: The 1D model of the water cavitation tube problem.

Phase	α	p[Pa]	ρ[kg/m^3]
liquid	0.99	10^5	1150
vapour	0.01	10^5	0.63

Table 6.1: Initial conditions for the water cavitation tube problem, based on the numerical experiment done by Pelanti and Shyue.

Phase	γ	π[Pa]	q[J/kg]	q'[J/kg/K]	C_v[J/kg/K]
liquid	2.35	10^9	-1167×10^3	0	1816
vapour	1.43	0	2030×10^3	-23.4×10^3	1040

Table 6.2: Thermodynamic coefficients for the water cavitation tube problem, based on the numerical experiment done by Pelanti and Shyue.

In the six-equation model of Pelanti and Shyue an equilibrium of the velocity is assumed, so there is only one mixture velocity u, whereas in the seven-equation model there is a velocity of the vapour u_v and a velocity of the liquid u_l. To compensate this in the seven-equation model, a strong relaxation of the velocity is applied in all simulations. The results are compared for the mechanical relaxation, i.e. p relaxation, the mechanical and thermal relaxation, i.e. p, T relaxation and for mechanical and thermodynamical relaxation, i.e. p, T, g relaxation, where g stands for Gibbs free energy and the relaxation of g represents the mass transfer between the two phases. In the simulations of Pelanti and Shyue, instantaneous relaxation is implemented. So for the seven-equation simulation the timescales are chosen small for the different relaxation terms, to retrieve almost instantaneous relaxation in the model. $\tau_u = 10^{-12}$ s, $\tau_p = 10^{-12}$ s, $\tau_T = 10^{-12}$ s and $\tau_g = 10^{-7}$ s.

At $t = 3.2$ ms the vapour fraction α_v, the mean pressure p and mean velocity u, which are given by

$$p = \alpha_v p_v + \alpha_l p_l \tag{6.1}$$

$$u = \frac{\alpha_v \rho_v u_v + \alpha_l \rho_l u_l}{\alpha_v \rho_v + \alpha_l \rho_l}, \tag{6.2}$$

obtained with the Baer-Nunziato model are shown in the figures below and compared with the results of Pelanti and Shyue.

For the generation of vapour in the cavitation of liquid water, that is the transfer from liquid water to water in vapour phase, the mass transfer plays a major role. When looking at the results for the vapour fraction in Figure 6.2, it is clear that when only the relaxation of p and p, T is applied the peak that represents the volume fraction of the vapour reaches a value just below 0.15. When the relaxation of g is added the volume fraction reaches almost the value of 0.3. In the simulation of Pelanti and Shyue the same difference is seen.

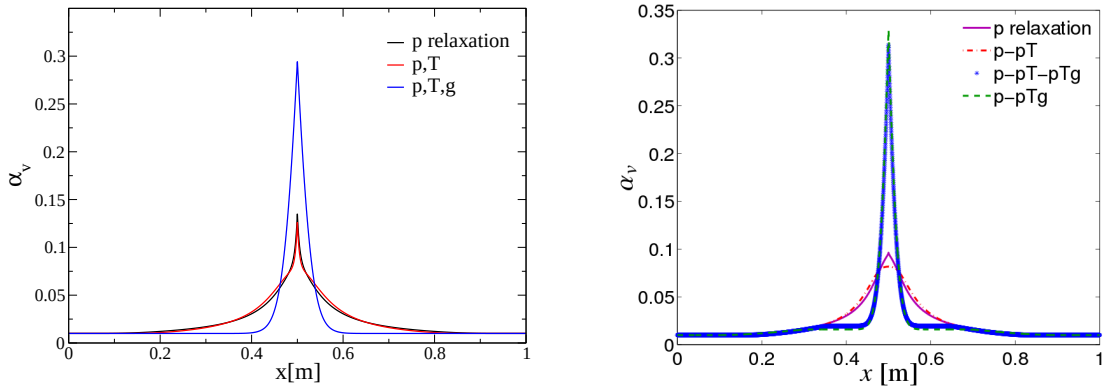

Figure 6.2: Results of the vapour volume fraction at $t = 3.2$ ms, left using the Baer-Nunziato model with three different relaxation terms, right the results of Pelanti and Shyue.

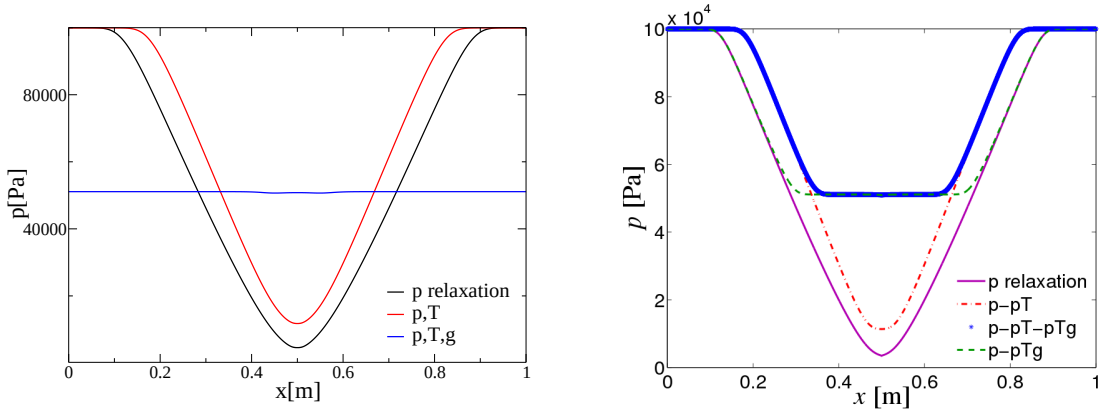

Figure 6.3: Results of the pressure at $t = 3.2$ ms: left using the Baer-Nunziato model with three different relaxation options, right the results of Pelanti and Shyue.

In the results of the pressure, Figure 6.3, a difference is visible. In the Baer-Nunziato model with p, T, g relaxation a difference can be observed at the ends of the pipe. This is probably caused by an additional condition that is used by M. Pelanti and K.-M. Shyue, namely that the g relaxation will only be applied in the case that $\epsilon_1 \leq \alpha_l \leq 1 - \epsilon_1$ and $T_v < T_{sat}(p_{eq})$, with $\epsilon_1 = 10^{-4}$, which they call the liquid-vapour interface location. The results generated with the Baer-Nunziato model show that in the entire pipe $\epsilon_1 \leq \alpha_l \leq 1 - \epsilon_1$ holds. So the g relaxation will only be applied in the case that $T_v < T_{sat}(p_{eq})$. The temperature at time $t = 3.2$ ms is given in Figure 6.4. In the simulation of Pelanti and Shyue the value of $T_{sat}(p_{eq})$ is most likely close to the initial temperature, 354.7 K. In this case the condition $T_v < T_{sat}(p_{eq}) = 354.7$ K holds between about $x = 0.4$ m and $x = 0.6$ m. This means that the g relaxation is only applied in this area for the six-equation model, whereas in the seven-equation simulation it is applied over the whole pipe. This would explain the difference between the results at the ends of the pipe.

This difference is also visible in Figure 6.5 where the velocity is shown. Here at the part where the pressure in the six-equation model is constant there is a difference between the six- and seven-equation results.

Although differences can be observed due to different implementations of the g relaxation, the

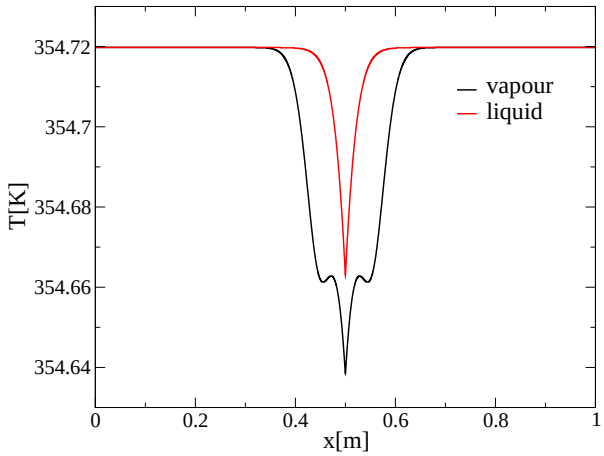

Figure 6.4: Temperature of the liquid and vapour in the pipe at $t = 3.2$ ms, using p, T, g relaxation.

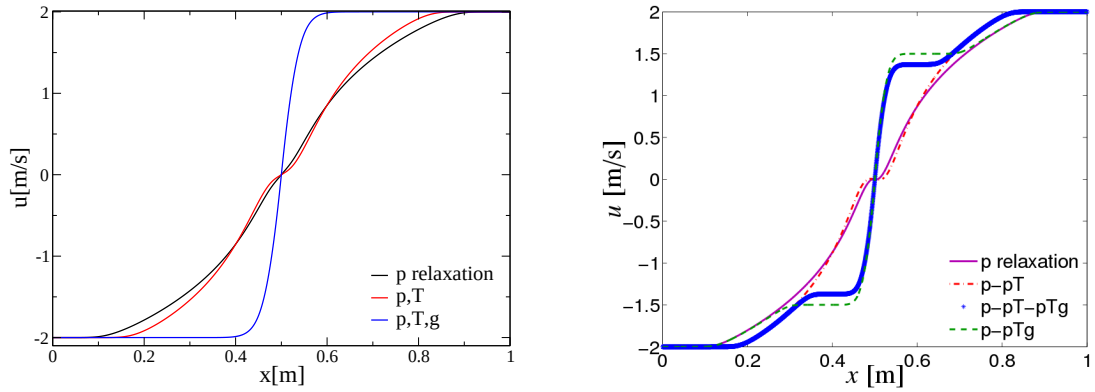

Figure 6.5: Results of the velocity at $t = 3.2$ ms: left using the Baer-Nunziato model with three different relaxation terms, right the results of Pelanti and Shyue.

current relaxation terms have similar influence on the pressure, velocity and mass fraction of the vapour as the relaxation terms used in the six-equation model of Pelanti and Shyue.

6.2 Edwards pipe experiment

The Edwards pipe experiment [25] is a fast depressurization of hot water in liquid phase generating much vapour. It is an important experiment for models that are used for the simulation of a Loss Of Coolant Accident (LOCA) in nuclear power plants. A LOCA is a hypothetical safety accident where (a part of) the cooling system stops working. This can cause damage in the core of the reactor. The Edwards pipe experiment includes a simple geometry. A horizontal pipe is considered of length $L = 4.097$ m and constant diameter $D = 0.07315$ m, which is closed at both ends. The initial temperature in the pipe is 515 K and the pressure is 70 bar, so that the pipe contains only water in liquid phase. The outside pressure is equal to the atmospheric pressure of 1 bar. At time $t = 0$ the pipe breaks at one end, and the cross section of the break is 12.5% smaller than the cross section of the pipe. When the pipe breaks, the depressurization causes the water to vaporise, such that at the end of the experiment the pipe contains vapour only. The 1D model is represented in Figure 6.6.

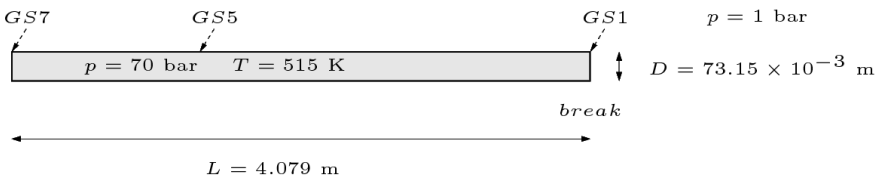

Figure 6.6: The 1D model of the Edwards pipe experiment.

During the experiment the average pressure $p = \alpha_v p_v + \alpha_l v_l$ in the pipe is measured at the break (this is point $GS1$) and near to the closed end of the pipe (location $GS7$). At 1.5 m from the closed end, at $GS5$, the vapour fraction α_v and the temperature T in the pipe are measured.

This experiment is simulated with Europlexus using a homogeneous four-equation model, called water model in Europlexus, and the seven-equation Baer-Nunziato model [11, 14] with the Rusanov scheme. For the seven-equation model, the new calibration of the thermodynamic coefficients is used. To validate the coefficients the results of the seven-equation model are compared with the water model, which uses the steam and water tables directly in the calculations. The results are also compared with the results of the WAHA code [26] and with the experimental results.

The WAHA code has been developed in a European project called WAHALoads [27] and is able to simulate two-phase water hammers. It uses a six-equation model thereby assuming a pressure equilibrium between the two phases.

The domain is split into two parts, the one-dimensional pipe and an outlet section, which is modelled as a tank in which a constant pressure equal to the atmospheric pressure of 1 bar is assumed. In the model a full area break is considered. The initial conditions are given in Table 6.3 and the thermodynamic coefficients of the problem are given in Table 6.4. The initial temperature is 515 K in both the pipe and the tank. For the seven-equation model the relaxation of the velocity, the mechanical relaxation and the thermodynamical relaxation are used, with the timescales $\tau_T = 10^{-12}$ s and $\tau_g = 5 \times 10^{-5}$ s. The timescales τ_u and τ_p are chosen automatically in the Europlexus simulation.

	Phase	α	p[Pa]	ρ[kg/m^3]
Pipe	liquid	$1 - 10^{-3}$	70×10^5	814.7195
	vapour	10^{-3}	70×10^5	33.1146
Tank	liquid	10^{-3}	10^5	806.9759
	vapour	$1 - 10^{-3}$	10^5	2.3297

Table 6.3: Initial conditions of the Edwards pipe experiment.

	Phase	γ	π[Pa]	q[J/kg]	q'[J/kg/K]	C_v[J/kg/K]
Pipe	liquid	1.5666	718960904	-1417310	8140.75	3053.63
	vapour	1.1294	422172	846047	-10993.18	3364.39
Tank	liquid	1.5666	718960904	-1417310	8140.75	3053.63
	vapour	1.1294	422172	846047	-10993.18	3364.39

Table 6.4: Thermodynamic coefficients for the Edwards pipe experiment.

For the simulation using the water model the Courant number of $\mathcal{C} = 0.7$ is the highest value for which the simulation is stable. For the seven-equation model an adaptive Courant number is used. In the first time step the Courant number is $\mathcal{C} = 0.01$, then each time step the size of the time step is doubled, until the Courant number of $\mathcal{C} = 0.8$ is reached. From that moment on a constant time step is used which corresponds to $\mathcal{C} = 0.8$.

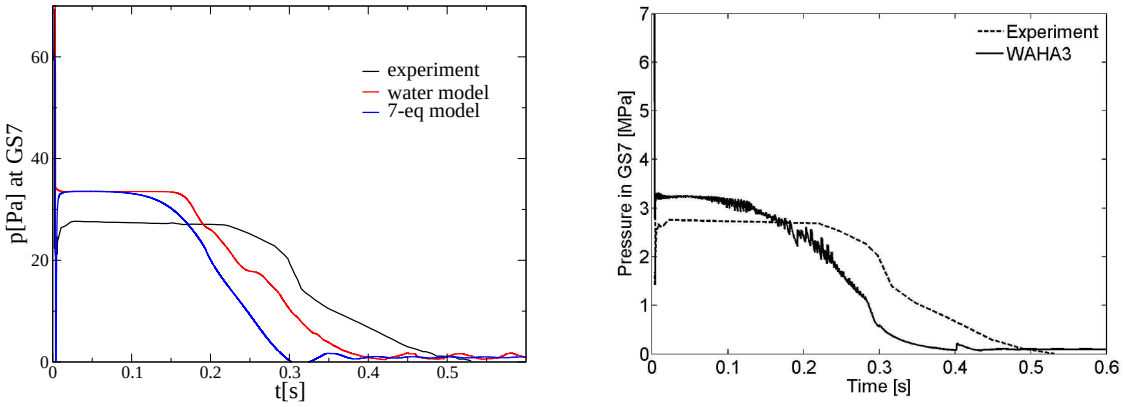

Figure 6.7: Results of the pressure over time using the water model and the Baer-Nunziato model with the Rusanov scheme at $GS7$. Left the Europlexus results, right the WAHA code results.

In the results of the pressure measured at the closed end of the pipe, at $GS7$, and given by Figure 6.7, the same plateau is visible for the seven-equation model and the water model. This means that with the new calibration of the thermodynamic coefficients the same saturation curve is retrieved as the curve based on the steam and water tables used in the water model. Furthermore the seven-equation model gives similar results as the six-equation model of the WAHA code.

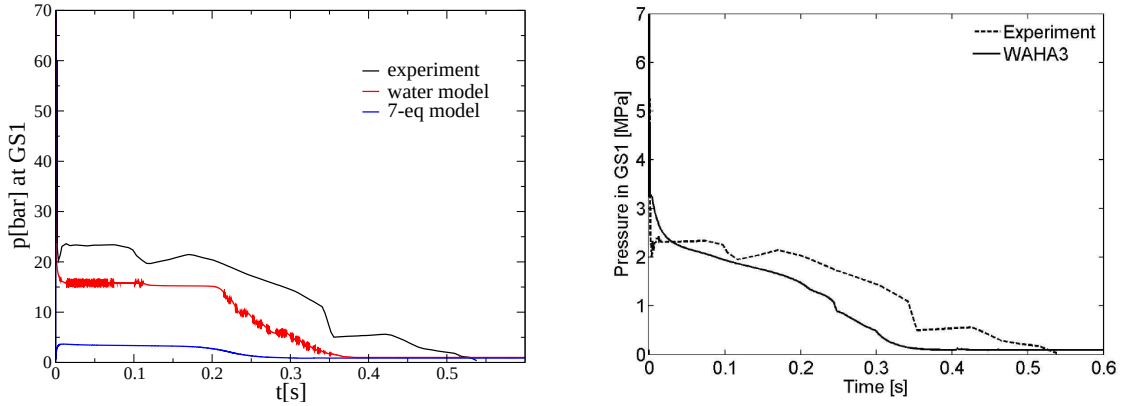

Figure 6.8: Results of the pressure over time using the water model and the Baer-Nunziato model with the Rusanov scheme at $GS1$. Left the Europlexus results, right the WAHA code results.

The difference between the model used in Europlexus and the model used in the WAHA code is the simplification of the partial break, 87.5%, to a full break (100%). Because the influence of the break is larger close to the break than at the closed end of the pipe, the results of the pressure at the break, see Figure 6.8, are very different, whereas the results at the closed end, see Figure 6.7, are very similar. To retrieve better results for the pressure the partial break should be included in the 1D simulation.

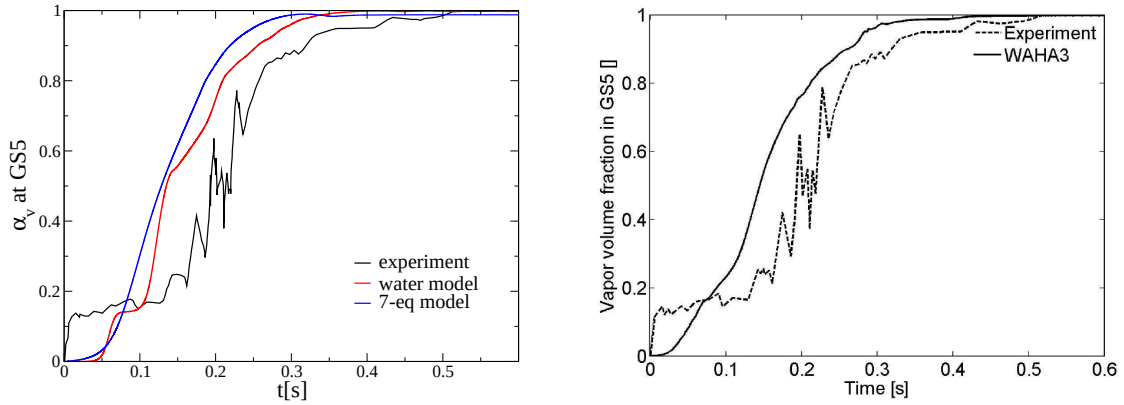

Figure 6.9: Results of the volume fraction of the vapour using the water model and the Baer-Nunziato model with the Rusanov scheme at $GS5$. Left the Europlexus results, right the WAHA code results.

In Figure 6.9 and Figure 6.10 again similar results are found with the seven-equation model and with the WAHA code. But the transition from full liquid to full vapour happens faster than in the physical experiment; indeed the volume fraction of the vapour increases faster and the temperature drops faster. One of the reasons for these differences could be caused by the delay in the measurement equipment.

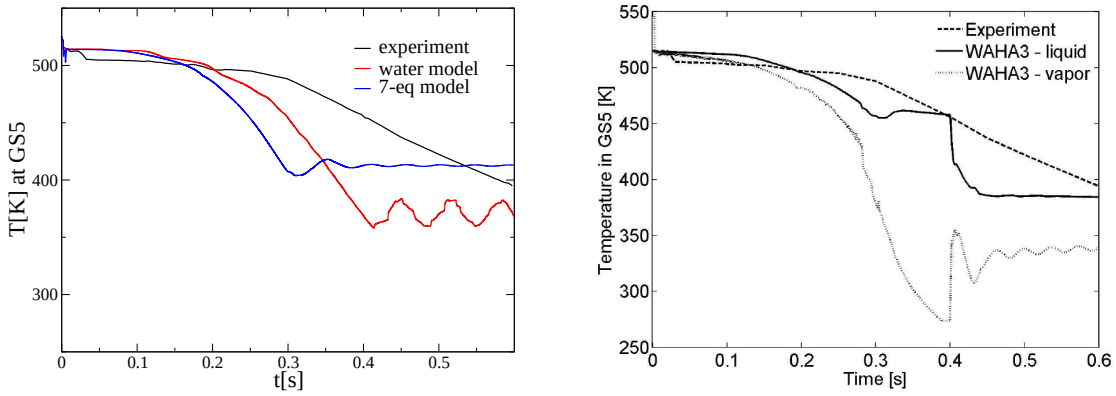

Figure 6.10: Results of the temperature using the water model and the Baer-Nunziato model with the Rusanov scheme at $GS5$. Left the Europlexus results, right the WAHA code results.

6.3 Cold water hammer test facility

The cold water hammer test facility [28] consists of a tank connected to a pipe with two 90° bends. The end of the pipe is blocked by a lid. Initially the pipe is split into two parts by a valve. In the left part, which is connected to the tank, the pressure is 1 bar. On the right side the pressure is decreased to the saturation pressure of 2.9×10^3 Pa at a temperature of 296.5 K. The fluid in the right part is in liquid phase for the main part, but the last 0.3 m below the lid is in vapour phase. This is reached by evacuating the air from the pipe, using a vacuum pump and decreasing the pressure to the saturation level at the initial temperature. The setup of the experiment is shown in Figure 6.11. The experiment has been built and carried out during the WAHALoads project [29].

Figure 6.11: Setup of the cold water hammer test facility experiment.

In the experiment the valve is opened almost instantaneously at $t = 0$ which creates a pressure wave travelling through the pipe. When the pressure wave reaches the vapour, the pressure in the vapour increases, exceeding the saturation pressure and the vapour collapses into liquid. This creates a pressure peak, the wave reflects and travels back into the direction of the tank, where it reflects again; this process continues.

With this experiment the thermal hydraulic part, i.e. the transition by sudden condensation of vapour to liquid, of the seven-equation model is assessed. To simulate the experiment the model is simplified to a 1D case where a straight rigid pipe attached to a tank is considered and the lid is modelled as a closed fixed end. So the fluid-structure interaction is neglected in this model. At 0.1 m from the closed end the mean pressure $p = \alpha_v p_v + \alpha_l p_l$ is measured; this point is called $MP1$. The 1D model is shown in Figure 6.12.

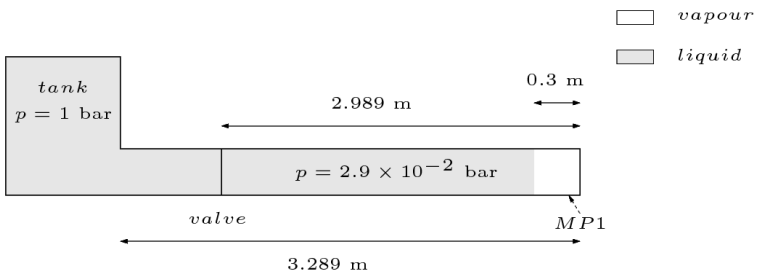

Figure 6.12: 1D model of the cold water hammer test facility.

The simulation with the seven-equation Baer-Nunziato model with the Rusanov scheme using the new calibration of the thermodynamic coefficients is compared with the simulation of the four-equation water model and the experimental values. In previous results [30] on a more com-

plex model, where the elbows in the pipe, the elasticity of the pipe and some fixation points of the structure are considered, the water model gave results which are very close to the experimental data. So here in the water model the elbows, support points of the structure and the elasticity of the pipe are added to the model. With this more detailed simulation the results of the pressure are measured at $MP1$ are retrieved. As can be seen in Figure 6.13, the results are close to the experimental data. Now for the simple 1D test case, where the elbows, support points and the elasticity of the pipe are neglected, the water model is used as a reference model. To test the calibration of the thermodynamic coefficients the values of the thermodynamic coefficients are adjusted to simulate the influence of the elasticity of the pipe on the celerity of the pressure waves.

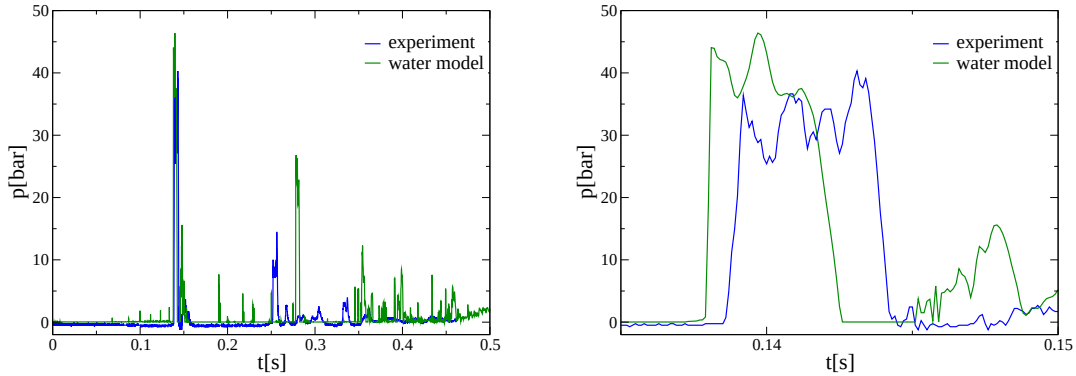

Figure 6.13: Pressure at $MP1$ using the 1D model including the elbows, support points and the elasticity of the pipe.

For the seven-equation model the thermodynamic coefficients for a rigid pipe that are used in the calculations are shown in Table 6.6. The timescales used for the relaxation terms are $\tau_g = 10^{-3}$ s, τ_u and τ_p are chosen automatically by the Europlexus simulation and there is no relaxation of the temperature.

Phase	γ	π[Pa]	q[J/kg]	q'[J/kg/K]	C_v[J/kg/K]
liquid	2.7981	79.4822×10^7	-1142335	31622.2	1494.98
vapour	1.3198	11.4901	1977373	1408.92	1446.89

Table 6.5: Thermodynamic coefficients in the pipe.

In Figure 6.13, the pressure profile is shown in the vapour part of the pipe, at $MP1$. It is clear that in the experiment the first pressure peak is much higher than the others; this means that it may cause the most damage to the structure. Therefore this first peak is the most important to examine, so the focus of the next images is on the first peak.

The first pressure peak is shown in Figure 6.14 for the simulation with the seven-equation model, the seven-equation model with adjusted thermodynamic coefficients to simulate the hoop elasticity of the pipe, the water model and the experimental data. Large differences in the arrival time and the height of the peak can be observed. The pressure peak of the simulation where the pressure wave speed of a rigid pipe is used, arrives earlier than in the experiment. When this speed is adjusted to mimic a flexible pipe the peak is closer to the experimental values. The arrival time is later, the peak is lower and the peak is wider. But still the experimental values are not exactly retrieved, because fluid-structure interaction is ignored. Therefore the simulation with the water model is used. In a 1D model including the elasticity and the elbow movements of the pipe,

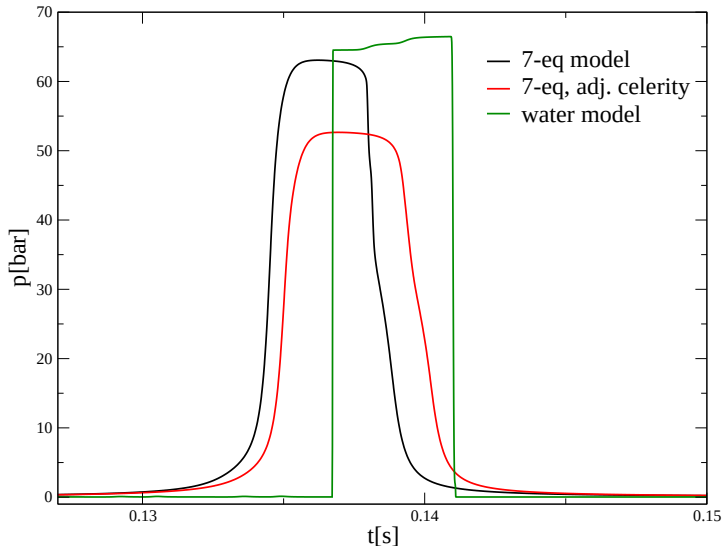

Figure 6.14: Results of the first pressure peak at $MP1$ over time.

the water model retrieves results very close to the experimental data, as shown in Figure 6.13. Because the pipe is considered rigid and straight in the simulation, the results are different from the experimental results.

Phase	γ	π[Pa]	η[J/kg]	η'[J/kg/K]	C_v[J/kg/K]
liquid	2.2449	68.6011×10^7	-1142327	23731.8	1863.31
vapour	1.3198	11.5408	1977350	1408.58	1446.94

Table 6.6: Thermodynamic coefficients with an adjustment on the celerity of the pressure wave.

Furthermore a difference in the speed of the wave can be observed between the different refinements of the grid when using the seven-equation model with the Rusanov scheme. The Rusanov scheme is a diffusive scheme which means that the interface between the water and the vapour is diffused, which results in a smaller full vapour part. This diffusion is shown in Figure 6.15, where the volume fraction of vapour is represented at the interface between the liquid and the vapour for different grid sizes. This is computed at $t = 1$ ms, so the pressure wave front did not yet reach the interface and the interface diffusion is only caused by the numerical scheme. So when the grid is refined, the diffusion of the interface becomes smaller, and thus the full vapour part is larger. The speed of the wave in vapour is zero, because the mixture will stay at vapour pressure (only the volume vapour fraction changes), therefore if the vapour part is smaller the pressure wave reaches $MP1$ faster. These results of the seven-equation model can be seen in Figure 6.16.

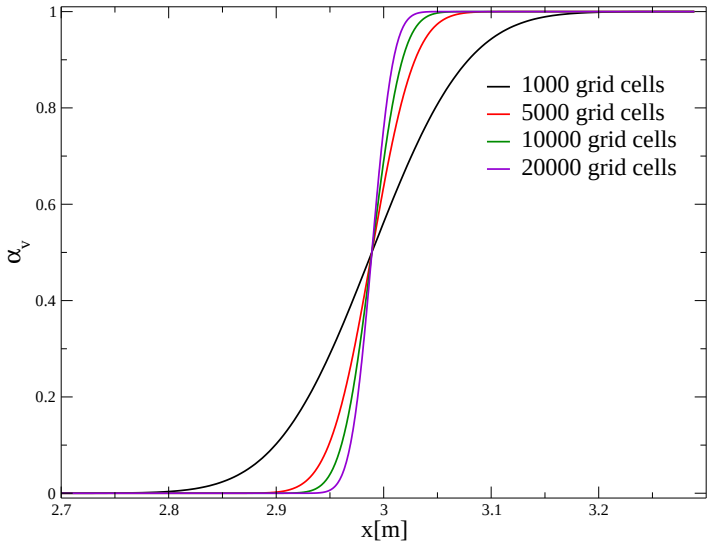

Figure 6.15: The volume fraction of the vapour at the interface between the liquid and the vapour at $t = 1$ ms, using the Rusanov scheme.

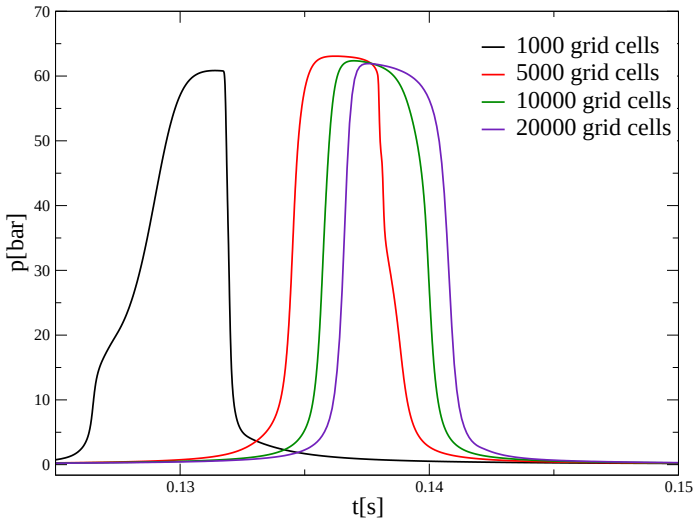

Figure 6.16: Pressure at $MP1$ for different refinements of the grid using the seven-equation model with the Rusanov scheme.

Chapter 7

Conclusions and recommendations

7.1 Conclusions

The seven-equation Baer-Nunziato model has been developed to simulate two-phase flows. It is a two-fluid model and uses seven equations with no equilibrium assumed between the two different phases that occur in the flow. A new calibration was proposed to approximate the coefficients of the stiffened gas equation of state, which are used in this model. In this thesis the goal was to assess the different parts of the seven-equation model and the new calibration of the stiffened gas coefficients. For this the model is assessed by simulating three different experiments. The water cavitation tube problem has been used to assess the relaxation terms in the seven-equation model, for the relaxation of pressure, temperature and chemical potential. The Edwards pipe experiment has been simulated to examine the new calibration of the equation of state coefficients and the seven-equation model. And finally the cold water hammer test facility was used to examine the influence of the elbows, fixed points and the fluid-structure interaction.

Overall the seven-equation model simulates the physical phenomena reasonably well. The propagation of the pressure waves, the cavitation due to pressure drop and the collapse of vapour cavities is well visible in the results of the different experiments. The HLLC scheme was in most cases not robust enough to perform the simulations; therefore the more robust, but more diffusive Rusanov scheme was used herein.

For the water cavitation tube problem similar results have been obtained with the different relaxation terms as those from the two-fluid six-equation model used by M. Pelanti and K.-M. Shyue. However, the predictions of the pressure when mass transfer between the two phases is included are different and this is caused by the different implementations of the chemical potential relaxation, or so called g relaxation.

In the Edwards pipe experiment the results of the seven-equation model are compared with the results of the water model, the experimental values and the results of the WAHA code. When comparing the results to the water model results, the same vapour saturation level is reached, which means that the new calibration of the equation of state reaches the same saturation curve. Furthermore, the results of the seven-equation model are similar to the results of the WAHA code, but the volume fraction of the vapour increases faster for the seven-equation model. So the differences between the seven-equation results and the experiment are caused by the mass transfer and the simplifications made in the model.

In the cold water hammer test facility results it can be seen that using the new calibration for the EOS coefficients, the celerity in the system can be easily adjusted to take into account the hoop elasticity of the pipe. This adjustment of the celerity resulted in an improvement of the

height, the width and the location of the pressure peak. Furthermore the results show that the fluid-structure interaction plays an important role. When this is neglected the pressure peaks caused by the water hammer are much higher and arrive earlier than in the physical experiment. The Rusanov scheme that is used in the computations with the seven-equation model appears to be very diffusive, which is visible when a refined grid is results in a better approximation.

7.2 Recommendations

For future work on the seven-equation model the focus should lie on the implementation of fluid-structure interaction. The seven-equation model with the Baer-Nunziato assumption yields good results when simple geometries are considered. In the case of more complex setups, the influence of structural deformations can be large and should be modelled to obtain the right height and location of the pressure peaks.

The mass transfer in the seven-equation model, or so called chemical potential relaxation should be improved. For this more experiments on the relaxation terms should be carried out. The convective scheme should also be improved, the Rusanov scheme is robust but very diffusive. Extending this to second-order accuracy will improve the results. The HLLC scheme is less diffusive, but not robust enough to simulate all experiments. More research on this scheme should be done to improve it, so that it can be used on more complex setups. Or research on alternative schemes should be done to find one which is robust on complex setups and less diffusive as the Rusanov scheme.

Furthermore the model should be assessed on more experiments to get a clearer picture on what parts of the model have the largest influence on the results. And what parts of the model are still missing.

Bibliography

[1] M.R. Baer and J.W. Nunziato. A two-phase mixture theory for the deflagration-to-detonation transition (ddt) in reactive granular materials. *International Journal of Multiphase Flow*, 12:861–889, 1986. 1

[2] N. Joukowsky. *Über den hydraulischen Stoss in Wasserleitungsröhren.* Mémoires de l'Académie Impériale des Sciences de St.-Pétersbourg, 1900. 3, 4

[3] L. Allievi. *Teoria del colpo dariete.* Atti Collegio Ing. Arch., 1913. (English translation by E.E. Halmos 1929), The theory of waterhammer. 3, 5

[4] L. Allievi. *Teoria generale del moto pertubato dell'acquanti tubi pressione.* Ann. Soc. Ing. Arch. Ithaliani., 1903. 3, 5

[5] S.K. Sinha, R.S. Vecchio, P.M. Bruck, T.C Esselman, G. Zysk, and D. Somrah. Condensation induced waterhammer in district steam distribution systems. In *ASME 2013 Pressure Vessels and Piping Conference*, pages V004T04A078–V004T04A078. American Society of Mechanical Engineers, 2013. 3

[6] M.S. Ghidaoui, M. Zhao, D.A. McInnis, and D.H. Axworthy. A review of water hammer theory and practice. *Applied Mechanics Reviews*, 58:49–76, 2005. 5

[7] D.J. Korteweg. Uber die fortplanzungsgeschwindigkeit des schalles in elastichen rohren. *Ann. Phys. Chemie*, 5:525–542, 1878. 6

[8] A.R. Simpson and E.B. Wylie. Large water-hammer pressures for column separation in pipelines. *Journal of Hydraulic Engineering*, 117(10):1310–1316, 1991. 6

[9] A.R. Simpson. *Large water hammer pressures due to column separation in sloping pipes (transient cavitation).* PhD thesis, The University of Michigan, 1986. 6

[10] A. Bergant, A.R. Simpson, and A.S. Tijsseling. Water hammer with column separation: A historical review. *Journal of Fluids and Structures*, 22:135–171, 2006. 9

[11] H. Lochon, F. Daude, P. Galon, and J.-M. Hérard. Computation of steam-water transients using a two-fluid seven-equation model. *Pressure Surges, Dublin, Ireland*, 2015. 11, 12, 31, 35

[12] F. Coquel, T. Gallouët, J.-M. Hérard, and N. Seguin. Closure laws for a two-fluid two-pressure model. *Comptes Rendus Mathematique*, 334:927–932, 2002. 12

[13] T. Gallouët, J.-M. Hérard, and N. Seguin. Numerical modeling of two-phase flows using the two-fluid two-pressure approach. *Mathematical Models and Methods in Applied Sciences*, 14:663–700, 2004. 12

[14] F. Crouzet, F. Daude, P. Galon, P. Helluy, J.-M. Hérard, O. Hurisse, and Y. Liu. Approximate solutions of the Baer-Nunziato model. *ESAIM: Proceedings*, 40:63–82, 2013. 12, 31, 35

[15] J.-M. Hérard and O. Hurisse. A fractional step method to compute a class of compressible gas-liquid flows. *Computers and Fluids*, 55:57–69, 2012. 13, 23

[16] O. Le Métayer, J. Massoni, and R. Saurel. Elaborating equations of state of a liquid and its vapor for two-phase flow models. *International Journal of Thermal Sciences*, 43:265–276, 2004. 15

[17] E. Blaud, p. Galon, and F. Daude. Introduction et validation d'un modèle de changement de phase dans le code de dynamique rapide Europlexus. Technical Report DEN/DANS/DM2S/SEMT/DYN/NT/14-015/A, CEA, 2014. 15

[18] http://www.iapws.org. The international association for the properties of water and steam, 2015. 15

[19] F. Daude and P. Galon. Développement d'un modèle diphasique à deux pressions dans Europlexus et vérifications numériques - partie convective. Technical Report H-T63-2012-01003-FR, EDF R&D, 2012. 24

[20] S.A. Tokareva and E.F. Toro. HLLC-type Riemann solver for the Baer-Nunziato equations of compressible two-phase flow. *Journal of Computational Physics*, 229:3573–3604, 2010. 24

[21] F. Daude, P. Galon, and A. Menasria. Intégration d'un schéma de type HLLC pour le modèle diphasique à deux pressions de type Baer & Nunziato dans Europlexus. Technical Report H-T63-2014-01350-FR, EDF R&D, 2014. 24

[22] D.W. Schwendeman, C.W. Wahle, and A.K. Kapila. The Riemann problem and the high-resolution Godunov method for a model of compressible two-phase flows. *Journal of Computational Physics*, 212:490–526, 2006. 24

[23] R. Saurel, F. Petitpas, and R. Abgrall. Modelling phase transition in metastable liquids: application to cavitating and flashing flows. *Journal of Fluid Mechanics*, 607:313–350, 2008. 31

[24] M. Pelanti and K.-M. Shyue. A mixture-energy-consistent six-equation two-phase numerical model for fluids with interfaces, cavitation and evaporation waves. *Journal of Computational Physics*, 259:331–357, 2014. 31

[25] A.R. Edwards and T.P. O'Brien. Sudies of phenomena connected with the depressurization of water reactors. Technical report, United Kingdom Atomic Energy Authority, Risley, Eng., 1970. 34

[26] J. Gale, I. Tiselj, and A. Horvat. Two fluid model of the WAHA code for simulations of water hammer transients. *Multiphase Science and Technology*, 20:291–322, 2008. 35

[27] M Giot et al. Two-phase flow water hammer transients and induced loads on materials and structures of nuclear power plants. *WAHALoads Project Description*, 2004. 35

[28] E. Altstadt, H. Carl, H.-M. Prasser, and R. Weiss. Fluid-structure interaction during artificially induced water hammers in a tube with bend-experiments and analyses. *Multiphase Sci. Technol.*, 20:213–238, 2008. 37

[29] M. Giot, H.M. Prasser, A. Dudlik, G. Ezsol, M. Habip, H. Lemonnier, I. Tiselj, F. Castrillo, W. Van Hove, R. Perezagua, and S. Potapov. Two-phase flow water hammer transients and induced loads on materials and structures of nuclear power plants (WAHALoads). Technical report, contract FIKS-CT-2000-00106, 2000. 37

[30] F. Daude and J. Delplace. Modélisation d'un coup de bélier de jonction de colonnes d'eau avec le code de dynamique rapide Europlexus. Technical Report H-T63-2014-00346-FR, EDF R&D, 2014. 38

Appendix A

Calculations and results

A.1 Simpson experiment

To get an understanding of how water hammers occur the Joukowsky formula (2.18) is used to calculate the pressure history in the two-phase Simpson experiment. The calculations are shown in Table A.1 and the corresponding results in Table A.2.

Time	Calculations
$t = 0$	$p_{new} - p_0 = \rho(-c)(0 - u_0)$ $p_{new} = p_1 = p_0 + \Delta p$, with $\Delta p = \rho c u_0$
$t = L/c$	$p_0 - p_1 = \rho c(u_{new} - u_0)$ $u_{new} = -\frac{\Delta p}{\rho c} = -u_0$
$t = 2L/c$	$p_{new} - p_0 = \rho(-c)(0 + u_0)$ $p_{new} = p_0 - \Delta p < p_{sat},\ p_{new} = p_{sat}$
$t = 3L/c$	$p_0 - p_{sat} = \Delta p_1 = \rho c(u_{new} - 0),\ \Delta p > \Delta p_1$ $u_{new} = \Delta p_1/\rho c < u_0$
$t = 4L/c$	$p_{sat} - p_0 = \rho(-c)(u_{new} - u_1)$ $u_{new} = 2u_1$, left of the vapour bubble
$t = 4L/c + \varepsilon$	collapse of the vapour bubble $p_{new} = p_2 = p_{sat} + \Delta p_2$, with Δp_2 the impact of the collapse, taken from the experiment
$t = 5L/c$	$p_0 - p_{sat} = \Delta p_1 = \rho c(u_{new} - 2u_1)$ $u_{new} = 3u_1$
	$p = p_0 + \Delta p_2,\ u = u_1$
$t = 5L/c + \varepsilon$	$p_0 - (p_0 + \Delta p_2) = \rho c(u_{new} - u_1)$ $u_{new} = -\frac{\Delta p_2}{\rho c} + u_1 = u_1 - u_2 < 0$
$t = 6L/c$	$p_{new} - (p_0 + \Delta p_2) = \rho(-c)(0 - u_1)$ $p_{new} = p_3 = p_0 + \Delta p_1 + \Delta p_2$
	$p = p_0 + \Delta p_1,\ u = -u_2$
$t = 6L/c + \varepsilon$	$p_{new} - (p_0 + \Delta p_1) = \rho(-c)(0 + u_2)$ $p_{new} = p_4 = p_0 + \Delta p_1 - \Delta p_2$
$t = 7L/c$	$p_0 - (p_0 + \Delta p_1) = \rho c(u_{new} + u_2)$ $u_{new} = -u_1 - u_2$

Table A.1: Calculations of the two-phase Simpson experiment.

Time	Point A	Point B
$t \leq 0$	$p = p_0$	$u = u_0$
$0 < t < L/c$	$p = p_1 = p_0 + \Delta p$	$u = u_0$
$L/c < t < 2L/c$	$p = p_1 = p_0 + \Delta p$	$u = -u_0$
$2L/c < t < 3L/c$	$p = p_{sat}$	$u = -u_0$
$3L/c < t < 4L/c + \varepsilon$	$p = p_{sat}$	$u = u_1$
$4L/c + \varepsilon < t < 5L/c$	$p = p_2 = p_{sat} + \Delta p_2$	$u = u_1$
$5L/c < t < 5L/c + \varepsilon$	$p = p_2 = p_{sat} + \Delta p_2$	$u = 3u_1$
$5L/c + \varepsilon < t < 6L/c$	$p = p_2 = p_{sat} + \Delta p_2$	$u = u_1 - u_2$
$6L/c < t < 6L/c + \varepsilon$	$p = p_3 = p_0 + \Delta p_1 + \Delta p_2$	$u = u_1 - u_2$
$6L/c + \varepsilon < t < 7L/c$	$p = p_4 = p_0 + \Delta p_1 - \Delta p_2$	$u = u_1 - u_2$
$7L/c < t < 7L/c + \varepsilon$	$p = p_4 = p_0 + \Delta p_1 - \Delta p_2$	$u = -u_1 - u_2$

Table A.2: Results of the two-phase Simpson experiment.

Appendix B

List of symbols

A	cross section of the pipe
c	speed of sound
$\tilde{c}$	speed of sound, with adjustments to account for the elasticity of the pipe
c_k	speed of sound in phase k
$C_{p,k}$	specific isobaric heat capacity of phase k
$C_{v,k}$	specific isochoric heat capacity of phase k
d	thickness of the pipe wall
D	inner diameter of the pipe
D_k	drag relaxation term of phase k
E	Young's modulus
e_k	specific total energy of phase k
g_k	Gibbs free energy of phase k
$\mathcal{H}$	$\frac{u_1 u_2}{2}$
h_k	specific enthalpy
j	phase, $j \in \{1, 2\}$, representing liquid if $j = 2$ or vapour when $j = 1$
k	phase, $k \in \{1, 2\}$, representing liquid if $k = 2$ or vapour when $k = 1$
K	bulk modulus
m_k	$\alpha_k \rho_k$ partial mass of phase k
p	absolute pressure
p_k	pressure of phase k
p_{sat}	vapour pressure
q_k	reference energy of the stiffened gas equation of state for phase k
q'_k	reference entropy of the stiffened gas equation of state for phase k
Q_k	heat transfer of phase k
s_k	specific entropy
$(S_k)_K$	wave speeds present in the Riemann problem where $K \in \{L, M, R\}$ for phase k
T_k	absolute temperature of phase k
T_{ref}	reference temperature
u	velocity
$\mathcal{U}$	$\frac{u_1 + u_2}{2}$
u_k	velocity of phase k
α_k	volume fraction of phase k
γ_k	specific heat ratio
Γ_k	mass transfer term of phase k
ε_k	specific internal energy of phase k
Λ_k	relaxation term consisting of the drag term and mass transfer of phase k
π_k	reference pressure of the stiffened gas equation of state for phase k
ρ	density

ρ_k	density of phase k
τ_ξ	timescale of the relaxation of ξ, where $\xi \in \{p, \mu, u, T\}$
φ	seven variables $\{\alpha_k, m_k, u_k, e_k\}$ where $\alpha_1 + \alpha_2 = 1$
Φ_k	pressure relaxation term of phase k
Ψ_k	relaxation term consisting of the heat transfer, the drag term, the mass transfer and the pressure term of phase k
colour	values represented in the colour green are retrieved from the water and steam tables